NTNU

Norwegian University of
Science and Technology

Charged Particle Motion in Turbulent Magnetic Fields

Kristian Joten Andersen

Project report

Submission date: 19.12.2016

Project supervisor: Prof. Michael Kachelrieß

Norwegian University of Science and Technology

Department of Physics

Preface

This report is written as part of my project assignment buliding up for my Master of Science in Astrophysics. It is worth 15 ECTS credits and is being completed at the Norwegian University of Science and Technology, NTNU. The work has been done under the supervision of Prof. Michael Kachelrieß at the Department of Physics.

I would like to thank Prof. Michael Kachelrieß for providing me with the interesting project. It has been both a rewarding and challenging task to work on. Also, I would like to thank him for his patience with me and his indispensable help in finding helpful written books and articles on the topic, and for helpful critique while writing this report.

Trondheim, 2016-12-19

Kristian Joten Andersen

Abstract

This report presents an analysis of deflection angles of very high energy charged particles particles propagating through randomly generated turbulent magnetic fields that are homogeneous and isotropic. The magnetic fields are modeled as a superposition of discrete Fourier modes with isotropically distributed wavevectors $\boldsymbol{k}$ logarithmically distributed in spatial frequency. We clarify a dispute in the literature and show under which conditions the algorithm used generates isotropic magnetic. The generated fields follow power spectra $E(k) \sim k^{-\gamma}$, and fields following Kolmogorov turbulence ($\gamma = 5/3$) are found to be approximately isotropic with 500 modes per decade of k-values. This number is found to increase with the spectral index γ. The analysis of the deflection angles utilizes a numerical simulation that integrates the trajectories of an ensemble of test particles from which the deflection angles based on the particle velocities are obtained. The deflection angles of particle motion with propagation length much shorter than the correlation length of the magnetic fields are found to be consistent with values deduced from constant magnetic fields. For propagation lengths much greater than the magnetic field correlation length the deflection angles are found to be smaller than the values predicted by diffusion in angle, i.e. random walk of small deflections.

Contents

Chapter 1

Introduction

1.1 Background

> "Magnetic fields are ubiquitous in the Universe. Wherever we have the means of observing them, they are present." (Durrer and Neronov (2013, p. 1))

Magnetic fields are everywhere, in stars, in our solar system, in the Milky Way, in other galaxies, in galaxy clusters and other structures in the Universe (Durrer and Neronov, 2013, p. 1-2). Depending on the source, the magnetic fields can be small or huge in extension and/or strength. The largest magnetic fields on the distance scale are the weak magnetic fields found in galaxies and galaxy clusters, with extensions of 10^{-2} to 1 Mpc; the largest of these being the Extragalactic Magnetic Fields (EGMF). While magnetic fields of smaller scales dissipate their energy into plasma motion over time, the largest fields might not have time to do so and therefore they conserve their strength on time scales comparable to the age of the Universe (Durrer and Neronov, 2013, p. 2). The generation of the EGMFs will not be discussed in this report, but is covered extensively in Durrer and Neronov (2013, chapter 3). Usually they are created due to motion in the cosmic plasma (Giacalone and Jokipii, 1999; Durrer and Neronov, 2013).

Knowing the strength and structure of the EGMFs is of high importance in order to understand our observations of the Universe. The Universe is full of ionized particles with whom the the magnetic fields interact through the Lorentz force. This in turn leads to deflections of the particles as well as to the emission of synchrotron radiation. In addition, the Universe is full of photons with whom the ionized particles also may interact, either through pair production or annihilation, or normal or inverse Compton scattering. In the case of very high energy (VHE) photons, pair production of electrons and positrons through interaction with extragalactic background light (EBL), followed by inverse compton (IC) scattering of e^-/e^+ with EBL, create electromagnetic cascades (EMC) (Neronov et al., 2010, p. 1)(Bergström and Goobar, 2004, p. 129-132). The photons created by these EMCs are observable, but their brightness profile will depend on the structure and strength of the EGMF in which the EMC took place.

Finding the structure and calculating or measuring the strength of a EGMF is a difficult challenge. One is not able to measure the direction and strength directly with today's technology, of obvious reasons such as having to leave the galaxy and sample the field at many different location spanning several kpc, preferably at the same time. Instead one need to look at observations presumably caused by the EGMF. The problem is that all effects (e.g. synchrotron radiation or

Faraday rotation) studied to calculate the magnetic fields use proto-electron density (e.g. see Durrer and Neronov, 2013). If the density is small, e.g. as it is in voids and extragalactic space, the effects are so weak that the fields can not be measured. Also, in the observations the EGMF strength is normally coupled with the structure of the EGMF model. In other words one only find constraints on the EGMF strength based on the model used. A possible observation that can be used to find constraints on the EGMF strength and structure is presented in Neronov et al. (2010), where Monte-Carlo simulations are used to compute the brightness profile in the GeV spectrum of "jets" from TeV blazars, i.e. active galaxies (active galactic nuclei, AGN). The article considers a turbulent model for the EGMF and computes brightness profiles of blazar "jets" for different values of the EGMF strength.

It is common to model the EGMF as a turbulent field (e.g. see Giacalone and Jokipii, 1999; Harari et al., 2002; Taylor et al., 2010). The largest magnetic fields, i.e. the EGMFs, also conserve their strength over large time scales (Durrer and Neronov, 2013, p. 2), although the magnetic field changes. The effects of the EGMF on cosmic rays (CR), i.e. VHE charged particles and photons, are themselves of a certain time scale. If the time scale of the change in the magnetic field is much larger than that of the interaction with the CR, the EGMF can be presumed to be *static* w.r.t. the CR (Giacalone and Jokipii, 1999, p. 205). In addition, the cosmic plasmas are generally irregular and turbulent (Giacalone and Jokipii, 1999, p. 205) which in turn makes the magnetic field irregular and turbulent. For this the EGMF will be modelled as a static turbulent magnetic field in this report. This leads to simplifications which will be shown later in the report.

A computational algorithm for the generation of a turbulent magnetic field is presented in the article by Giacalone and Jokipii (1994) and has been used in other papers since (e.g. see Neronov et al., 2010). It computes a isotropic and homogeneous magnetic field with zero mean, which is presumed to be the properties of the EGMF by the articles it is used. In contradiction to Giacalone and Jokipii (1994) in the article by Tautz (2012) the computation algorithm is criticized not to give an isotropic field. If this is the case then it may have implications on work done using this algorithm. A clarification of this disagreement is therefore of high interest.

Problem Formulation

In this report I will look at the following:

1. Giacalone and Jokipii (1994) and Tautz (2012) consider the same algorithm for numerically creating a turbulent magnetic field, but come to different conclusions considering the isotropy of the created field. I will analyse the arguments of both articles and clarify the definitions and parameters of the algorithm to find an answer to whether the resulting field is isotropic or not. Further, if the resulting field proves to be isotropic, what would the correlation length of such a field be? How does the correlation length compare to a continuous field with equal power spectrum (see Harari et al., 2002)?

2. Given the above; in a weak field limit, what would the deflection angle of a charged particle with very high energy (i.e. highly relativistic) over the distance of several correlation lengths be, so that details of the realization are washed out?

The first point is of interest for physicists who want to implement a turbulent magnetic field model in mostly any numerical computation. When considering the disagreement between Giacalone and Jokipii (1994) and Tautz (2012), it is of high interest to know whether the algorithm

works as it is supposed to, as it has been implemented in other numerical computations since the publication of the article by Giacalone and Jokipii (1994) (e.g. see Giacalone and Jokipii, 1999; Neronov et al., 2010). If the algorithm proves to be wrong, many results in these articles might have a systematic error that they're unaware of.

As for the second point, the interest lies mostly with astrophysicists who wants to look at charged particle motion and its application for highly relativistic particles, e.g. EMCs in the EGMF if one applies a turbulent model. The last can be used to simulate possible brightness profiles for VHE sources in the Universe (e.g. see Neronov et al., 2010).

1.2 Objectives

The main objectives of this assignment project are

1. Analyze the algorithm in Giacalone and Jokipii (1994) and Tautz (2012) for computing turbulent magnetic fields and examine if the resulting field has the following properties: (i) is isotropic, (ii) follows a given power law, (iii) has zero divergence and mean value, (iv) has a given mean strength, i.e. constant mean energy density on scales larger than the largest turbulence structures?

2. Calculate the correlation length of the computed turbulent fields from the algorithm in Giacalone and Jokipii (1994) and compare the results to analytical values of a turbulent field with continuous k-values described in Harari et al. (2002, ch. 2).

3. Use numerical computation to calculate the deflection angle of VHE electron motion through the computed turbulent magnetic fields, then compare the deflection angles to values from analytical formulae (Caprini and Gabici, 2015).

1.3 Approach

All objectives in this report will be solved using numerical computation. For the first objective the established algorithm for creating turbulent magnetic fields (see Giacalone and Jokipii, 1994; Tautz, 2012) will be analyzed. Then using Monte-Carlo (MC) computation, the fields will be computed and checked for isotropy and magnetic field strength. For the second objective, MC computation and Simpson's rule integration is used to calculate the correlation length of the magnetic fields. To solve the third objective, an adaptive Runge-Kutta solver will be used to compute particle trajectories on distance scales of order of the calculated correlation lengths from the second objective.

1.4 Structure of the Report

The rest of the report is structured as follows. Chapter 2 gives an introduction to general turbulent magnetic field theory, before the numerical algorithm from Giacalone and Jokipii (1994) and Tautz (2012) is presented and analyzed. The disagreement of the isotropy will be handled in subsection 2.2.2. Chapter 3 introduces the theory of charged particle motion and the numerical

methods used to calculate the deflection of the propagation. In Chapter 4 the results from the computations are presented and discussed, following the order of the objectives presented earlier in this chapter. At last chapter 5 gives a short summary of the most important results found in this report.

Chapter 2

Turbulent Magnetic Fields

2.1 General Theory

An electromagnetic system in vacuum always needs to satisfy the Maxwell equations

$$\nabla \cdot \boldsymbol{E} = \frac{\rho}{\epsilon_0}, \tag{2.1}$$

$$\nabla \cdot \boldsymbol{B} = 0, \tag{2.2}$$

$$\nabla \times \boldsymbol{E} = -\frac{\partial \boldsymbol{B}}{\partial t}, \tag{2.3}$$

$$\nabla \times \boldsymbol{B} = \mu_0 \left(\boldsymbol{J} + \epsilon_0 \frac{\partial \boldsymbol{E}}{\partial t} \right), \tag{2.4}$$

where $\boldsymbol{E}$ and $\boldsymbol{B}$ is the electric and magnetic field, ρ is the total electric charge density, $\boldsymbol{J}$ is the total current density, and ϵ_0 and μ_0 is respectively the electic permittivity and the magnetic permeability in vacuum. In the case of a static magnetic field, equation (2.3) becomes zero, i.e. there are no induced voltages due to the magnetic field. Further, a constant magnetic field implies that the r.h.s. of equation (2.4) must be constant, where the stable solution is a constant electric field and a constant current density. When considering a magnetic field, equation (2.2) is the most important, as it shows that the divergence of the magnetic field is independent of the electric field and is always zero.

2.1.1 Magnetic Turbulence

Hydrodynamic turbulence is normally modelled as eddy currents of different scale sizes. The energy density contained in each scale size of the eddies, i.e. the turbulence, is assumed to follow a power spectrum given by

$$E(L) \propto L^{\gamma}, \tag{2.5}$$

where L is the scale size of the eddies, $E(L)$ is the energy of that scale size, and γ is called the spectral index. In magnetic turbulence one look at magnetic eddies each with its own strength $B(L)$. As the energy density of a magnetic field is proportional to the magnetic field strength squared, and using the spatial frequency, i.e. the wavenumber, of the eddies $k = 2\pi/\lambda$ where

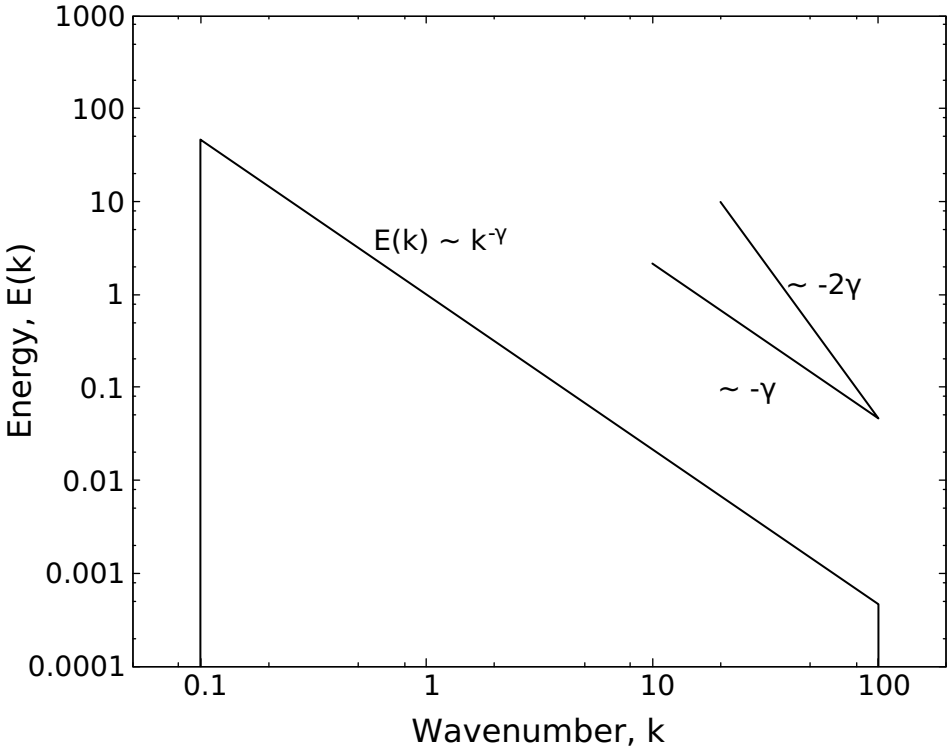

Figure 2.1: The figure shows a logarithmic energy spectrum, analogous to equation (2.6), of a turbulent magnetic field consisting of magnetic eddies of different scale sizes. E is the energy of each eddy with wavenumber $k = 2\pi/L$, where L is the scale size. The power spectrum follows a spectral index $\gamma = 5/3$, equivalent to Kolmogorov turbulence, between k-values of 0.1 and 100. The angle to the right shows the inclination of the graph if the spectral index were to be doubled. Note: The figure only shows the relation between E and k, i.e. $E = C \cdot k^{-\gamma}$ where C is a constant here set to 1. Any units of E or k is therefore not given as they would normally depend on C.

$\lambda = L$ one gets

$$E(k) \propto B^2(k) \propto k^{-\gamma}. \tag{2.6}$$

Figure 2.1 shows a possible power spectrum of a turbulent magnetic field following this relation.

One can model a turbulent magnetic field as a Gaussian random field with zero mean and a root mean square value B_{rms} using superposition of Fourier modes (i.e. plane waves) as

$$B_i(\boldsymbol{x}) = \int \frac{\mathrm{d}^3 k}{(2\pi)^3} B_i(\boldsymbol{k}) e^{i(\boldsymbol{k}\cdot\boldsymbol{x}+\phi_i(\boldsymbol{k}))}, \tag{2.7}$$

where $B_i(\boldsymbol{x})$ is the magnetic field component in direction of $\hat{\boldsymbol{e}}_i$, and $\phi(\boldsymbol{k})$ are random phases (Harari et al., 2002, p. 3). Note that $|\boldsymbol{k}| = k$ and all $\boldsymbol{k}$'s have random directions independent of each other. In order for this field to have zero divergence, see equation (2.2), the components $B_i(\boldsymbol{k})$ must be so that

$$\boldsymbol{B}(\boldsymbol{k}) \cdot \boldsymbol{k} = 0, \tag{2.8}$$

where

$$\boldsymbol{B}(\boldsymbol{k}) = B_x(\boldsymbol{k})\hat{\boldsymbol{e}}_x + B_y(\boldsymbol{k})\hat{\boldsymbol{e}}_y + B_z(\boldsymbol{k})\hat{\boldsymbol{e}}_z. \tag{2.9}$$

If the field is isotropic and homogeneous the random Fourier modes satisfy the relation

$$\langle \boldsymbol{B}(\boldsymbol{k}_i) \cdot \boldsymbol{B}^*(\boldsymbol{k}_j) \rangle = B^2(k)\delta_{ij}. \tag{2.10}$$

Further, this makes it so that the root mean square value is

$$B^2_{\text{rms}} \equiv \langle \boldsymbol{B}(\boldsymbol{x}) \cdot \boldsymbol{B}^*(\boldsymbol{x}) \rangle = \int B^2(k)\mathrm{d}k. \tag{2.11}$$

Using equation (2.6) and assuming the wavenumbers of the turbulence is constrained by the limits $k_{\text{min}} < k < k_{\text{max}}$ (i.e. scale sizes $L_{\text{min}} < L < L_{\text{max}}$), equation (2.11) gives the magnetic field strength of the model for each value of k to be

$$B^2(k) = B^2_{\text{rms}} k^{-\gamma} \frac{(\gamma-1)k_{\text{min}}^{\gamma-1}}{1-(k_{\text{min}}/k_{\text{max}})^{\gamma-1}}. \tag{2.12}$$

2.1.2 Correlation Length

Harari et al. (2002, p. 3) defines the magnetic field correlation length through

$$L_c B^2_{\text{rms}} \equiv \int_{-\infty}^{\infty} \mathrm{d}L \, \langle \boldsymbol{B}(0) \cdot \boldsymbol{B}(\boldsymbol{x}(L)) \rangle \,, \tag{2.13}$$

where $\boldsymbol{B}(0)$ is the magnetic field at a random position and $\boldsymbol{B}(\boldsymbol{x}(L))$ is the magnetic field at a position displaced by a distance L along a fixed direction. Note that this would only be a scalar quantity for an isotropic field, as the resulting correlation length otherwise would depend on the direction chosen. Assuming an isotropic and homogeneous field, inserting the magnetic field defined in equation (2.7) into equation (2.13) gives

$$L_c B^2_{\text{rms}} = \pi \int_0^{\infty} \frac{\mathrm{d}k}{k} B^2(k), \tag{2.14}$$

which after insertion of equation (2.12) results in

$$L_c = \frac{1}{2} L_{\text{max}} \frac{\gamma-1}{\gamma} \frac{1-(L_{\text{min}}/L_{\text{max}})^{\gamma}}{1-(L_{\text{min}}/L_{\text{max}})^{\gamma-1}}. \tag{2.15}$$

Here L_{min} and L_{max} are the constraints on the scale size of the magnetic eddies, as defined for equation (2.12), with the relation $k = 2\pi/L$. Note that $k_{\text{min}} \propto L^{-1}_{\text{max}}$, as with $k_{\text{max}} \propto L^{-1}_{\text{min}}$, so that $L_{\text{min}}/L_{\text{max}} = k_{\text{min}}/k_{\text{max}}$. One see that for a large value of γ ($\gamma \gg 1$) or a narrow-band ($L_{\text{min}} \sim L_{\text{max}}$) the correlation length $L_c \simeq L_{\text{max}}/2$. For a broad-band ($L_{\text{min}} \ll L_{\text{max}}$), the correlation length goes towards $L_c \simeq (\gamma-1)L_{\text{max}}/2\gamma$.

Defining the spatial correlation function

$$\xi_{ij}(|\boldsymbol{y}|) = \langle B_i(\boldsymbol{x}) B_j(\boldsymbol{x}+\boldsymbol{y}) \rangle \,, \tag{2.16}$$

where x and y are random and isotropic position vectors, and $B_i(\boldsymbol{x})$ is the magnetic field strength

in $\hat{\boldsymbol{e}}_i$ direction at position x. Further, using *Einsein summation convention*

$$\xi_{ii}(|\boldsymbol{y}|) = \langle \boldsymbol{B}(\boldsymbol{x}) \cdot \boldsymbol{B}(\boldsymbol{x}+\boldsymbol{y}) \rangle \,. \tag{2.17}$$

From equation (2.11) one get in the limit $|\boldsymbol{y}| = 0$ that $\xi_{ii}(0) = B^2_{\text{rms}}$ as one should expect. In the case of isotropic and homogeneous magnetic turbulence, equation (2.13) can be rewritten as

$$L_c B^2_{\text{rms}} = 2 \int_0^\infty \xi_{ii}(L)\, \mathrm{d}L, \tag{2.18}$$

where the relations $\boldsymbol{x}(-L) = -\boldsymbol{x}(L)$ and $\xi_{ii}(|\boldsymbol{x}|) = \xi_{ii}(|-\boldsymbol{x}|) = \xi_{ii}(L)$ are used.

2.2 Computational Algorithm

In order to compute a random turbulent magnetic field of the same form as the magnetic field in equation (2.7) this report follows the algorithm presented in Giacalone and Jokipii (1994). The algorithm in Giacalone and Jokipii (1994) computes a complex magnetic field through a superposition of Fourier modes, each with a random polarization and a random direction defined by two angles θ and ϕ. A three-dimensional realization of $\boldsymbol{B}(\boldsymbol{r})$ which satisfies equation (2.2) may be written

$$\boldsymbol{B}(\boldsymbol{r}) = \sum_{j=1}^{n_k} B(k_j) \boldsymbol{\zeta}_j e^{i(k_j z' + \beta_j)}, \tag{2.19}$$

where n_k is the number of modes, k_j is the the mode's wavenumber, and $B(k_j)$ is the amplitude of the respective mode and may be chosen to follow the desired power spectrum. $\boldsymbol{\zeta}_j$ is the polarization vector and is given by

$$\boldsymbol{\zeta}_j = \cos(\alpha_j)\hat{\boldsymbol{e}}_{x'} \pm i \sin(\alpha_j)\hat{\boldsymbol{e}}_{y'}. \tag{2.20}$$

Each wave propagates in its own z'-direction with polarization in the $x'y'$-plane, where the primed system is related to the unprimed system through the rotation

$$\boldsymbol{r'_{3D}} = R(\theta,\phi)\boldsymbol{r_{3D}}, \tag{2.21}$$

with rotation matrix

$$R(\theta,\phi) = \begin{pmatrix} \cos(\theta)\cos(\phi) & \cos(\theta)\sin(\phi) & -\sin(\theta) \\ -\sin(\phi) & \cos(\phi) & 0 \\ \sin(\theta)\cos(\phi) & \sin(\theta)\sin(\phi) & \cos(\theta) \end{pmatrix}, \tag{2.22}$$

where θ and ϕ are functions of k. It can easily be shown that the primed system is defined by orthonormal basis vectors. The phases α_j and β_j, and the sign $\pm$ in equation (2.20), chosen randomly, are responsible for the random polarization. Meanwhile the angles θ and ϕ gives the random propagation direction. This means that for any realization of the magnetic field, and

for each k, there are five random numbers:

$$0 \leq \theta(k) \leq \pi,$$

$$0 \leq \phi(k) < 2\pi,$$

$$0 \leq \alpha(k) < 2\pi,$$

$$0 \leq \beta(k) < 2\pi,$$

and the plus or minus sign ($s = \pm$). The probability distribution of these will be given in the subsection 2.2.2.

The wavenumbers k_j is set to be logarithmically distributed between $k_{\min}$ and $k_{\max}$ in order to give each decade in scale sizes equal weighting of k numbers. This is similar to an assumption for normal hydrodynamic turbulence, where eddies are modelled to transfer its energy into eddies of a smaller scale size with a constant scale ratio, resulting in logarithmically spaced scale sizes.

2.2.1 Normalization

The turbulent magnetic field strength should be normalized to the value B_{rms}. In this subsection the magnetic field is assumed to be isotropic as this simplifies the normalization. Equations (2.22) and (2.20) show that $|\boldsymbol{\zeta}_j| = 1$. Now, if for any pair $\{\boldsymbol{k}_j, \boldsymbol{k}_l\}$ the scale size of the magnetic field $L_{MF} \gg 2\pi/|k_j - k_l|$, it may be shown for the Fourier modes that

$$\langle (\boldsymbol{\zeta}_j e^{i(k_j z'_j + \beta_j)}) \cdot (\boldsymbol{\zeta}_l e^{i(k_l z'_l + \beta_l)})^* \rangle = \delta(\boldsymbol{k}_j - \boldsymbol{k}_l). \tag{2.23}$$

Using this result and inserting equation (2.19) into (2.11) one gets

$$B^2_{\text{rms}} = \sum_{j=1}^{n_k} B^2(k_j). \tag{2.24}$$

The desired power law for the turbulence is given by equation (2.6). Using the scale sizes of the Fourier modes one can rewrite the amplitude as

$$B(k) = B(k_{\min}) \left(\frac{k}{k_{\min}} \right)^{-\gamma/2}, \tag{2.25}$$

where $B(k_{\min})$ is the amplitude of the mode corresponding to the minimum wavenumber $k_{\min}$, i.e. the largest turbulent structure. Inserting equation (2.25) into (2.24) one gets

$$B^2(k_{\min}) = \frac{B^2_{\text{rms}}}{\sum_{k_j} \left(\frac{k_j}{k_{\min}} \right)^{-\gamma}}, \tag{2.26}$$

and the square root of the r.h.s. gives the normalized value for $B(k_{\min})$. In the case where the field is not isotropic, equation (2.11) does not simply result in equation (2.24), and each mean value of $\langle \boldsymbol{B}(\boldsymbol{k}_i) \cdot \boldsymbol{B}^*(\boldsymbol{k}_j) \rangle$ would have to be calculated.

The magnetic field should be real. On the contrary, the field created by equation (2.19), and presumably (2.7), is complex. In order to acquire a real field, one only has to take the real part of

the resulting field, but this will change the RMS value. Using $\boldsymbol{x}\cdot\boldsymbol{x}^* = \mathrm{Re}^2(\boldsymbol{x}) + \mathrm{Im}^2(\boldsymbol{x})$, equation (2.11) gives

$$B_{\mathrm{rms}}^2 = \langle \boldsymbol{B}(\boldsymbol{r})\cdot\boldsymbol{B}^*(\boldsymbol{r})\rangle = \langle \mathrm{Re}^2(\boldsymbol{B})\rangle + \langle \mathrm{Im}^2(\boldsymbol{B})\rangle\,. \tag{2.27}$$

In addition, $\langle \mathrm{Re}^2(\boldsymbol{B})\rangle = \langle \mathrm{Im}^2(\boldsymbol{B})\rangle$ which may be acquired by taking the mean square of the real and imaginary part of $\boldsymbol{\zeta}$ times the exponent. Now one simply gets

$$\langle \mathrm{Re}^2(\boldsymbol{B})\rangle = \frac{1}{2}B_{\mathrm{rms}}^2. \tag{2.28}$$

In order to make only the real part of the computed B-field to have a RMS value equal to B_{rms} one only needs to multiply $B(k_{\mathrm{min}})$ with $\sqrt{2}$. The new equations for the turbulent magnetic field would then be

$$\boldsymbol{B}(\boldsymbol{r}) = \mathrm{Re}\left\{\sum_{k_j} B(k_j)\boldsymbol{\zeta}_j e^{i(k_j z' + \beta_j)}\right\}, \tag{2.29}$$

$$B(k_{\mathrm{min}}) = B_{\mathrm{rms}}\left(\frac{2}{\sum_{k_j}\left(\frac{k_j}{k_{\mathrm{min}}}\right)^{-\gamma}}\right)^{1/2}, \tag{2.30}$$

with equation (2.25) staying the same.

2.2.2 Isotropy

It should be noted that the choice of the placement of the primed parameters in equations (2.19) and (2.20) is not the same as the placement in Giacalone and Jokipii (1994), but equals the placement in Tautz (2012) and other articles using the algorithm (e.g. see Giacalone and Jokipii, 1999). The reason to this lies in the isotropy as will now be shown. Note also that the algorithm only computes a discrete set of modes with different amplitudes. This means that in order for the set of $\boldsymbol{k}$ to be isotropic, one needs a large number of modes per decade of k values. In addition, if γ is large the difference in strength between the modes becomes even greater and the smallest k values dominate, i.e. the largest scale sizes, which in turn will require even more modes. Since the number of modes proportionally affects computation time, one would in principle want just enough modes to make the computed field approximately isotropic. We assume for now that the number of modes n_k is sufficiently large.

If the magnetic field is to be isotropic with zero mean, it must satisfy the following:

$$\langle \boldsymbol{B}(\boldsymbol{r})\rangle = \vec{\boldsymbol{0}}\,, \tag{2.31}$$

and

$$\langle |B_x(\boldsymbol{r})\hat{\boldsymbol{e}}_x|^2\rangle = \langle |B_y(\boldsymbol{r})\hat{\boldsymbol{e}}_y|^2\rangle = \langle |B_z(\boldsymbol{r})\hat{\boldsymbol{e}}_z|^2\rangle = \frac{1}{3}B_{\mathrm{rms}}^2. \tag{2.32}$$

Equation (2.31) is satisfied if for each k:

$$\langle \boldsymbol{\zeta}_j e^{i(k_j z' + \beta_j)}\rangle = 0. \tag{2.33}$$

Assuming the extent of the magnetic field is much larger than the largest magnetic eddies so that $e^{i(k_j z'+\beta_j)}$ completes many cycles, i.e. $k_j|z'|_{\max} \gg 2\pi$, then equation (2.33) is satisfied.

It can be shown that if the $\boldsymbol{k}$'s are isotropic, then so is $\boldsymbol{B}$. This will simultaneously give the distributions of the five random numbers $\alpha, \beta, \theta, \phi$, and the plus or minus sign. Since $\hat{\boldsymbol{k}} = \hat{\boldsymbol{z}}'$ and $\boldsymbol{k} = k\hat{\boldsymbol{k}}$, equations (2.21) and (2.22) give

$$\boldsymbol{k} = k\left(\sin(\theta)\cos(\phi)\hat{\boldsymbol{e}}_x + \sin(\theta)\sin(\phi)\hat{\boldsymbol{e}}_y + \cos(\theta)\hat{\boldsymbol{e}}_z\right). \tag{2.34}$$

If $\boldsymbol{k}$ is isotropic then, similar to equations (2.31) and (2.32), one need

$$\langle \boldsymbol{k} \rangle = \langle \sin(\theta)\cos(\phi) \rangle \hat{\boldsymbol{e}}_x + \langle \sin(\theta)\sin(\phi) \rangle \hat{\boldsymbol{e}}_y + \langle \cos(\theta) \rangle \hat{\boldsymbol{e}}_z = \vec{0}, \tag{2.35}$$

and

$$\langle \sin^2(\theta)\cos^2(\phi) \rangle = \langle \sin^2(\theta)\sin^2(\phi) \rangle = \langle \cos^2(\theta) \rangle = \frac{1}{3}, \tag{2.36}$$

where it is used that $|\boldsymbol{k}|^2 = k^2$. From the equation (2.36) it is clear that $\langle \cos^2(\theta) \rangle = 1/3 \implies \langle \sin^2(\theta) \rangle = 2/3$. The only probability distribution $p(\theta)$ satisfying this as well as zero mean over the interval $0 \leq \theta(k) \leq \pi$ is $p(\theta) = \sin(\theta)/2$. This require that $\langle \cos^2(\phi) \rangle = \langle \sin^2(\phi) \rangle = 1/2$ over the interval $0 \leq \phi(k) < 2\pi$ to satisfy equation (2.36), and requiring zero mean in (2.35) the only possible distribution is a flat distribution $p(\phi) = 1/2\pi$.

With this new-found isotropy for $\boldsymbol{k}$ and assuming that the magnetic field is much greater than the largest turbulence structures, i.e. one has a homogeneous field, equation (2.10) holds for the Fourier modes. Further using (2.11) and (2.19) one get for the components in equation (2.32)

$$\langle |B_l(\boldsymbol{r})\hat{\boldsymbol{e}}_l|^2 \rangle = \sum_{j=1}^{n_k} B^2(k_j) \left\langle \left| \left[\boldsymbol{\zeta}_j e^{i(k_j z'+\beta_j)} \right]_l \right|^2 \right\rangle, \tag{2.37}$$

where $\left[\boldsymbol{\zeta}_j e^{i(k_j z'+\beta_j)} \right]_l$ is the component of $\hat{\boldsymbol{B}}$ in $\hat{\boldsymbol{e}}_l$ direction. Now if the mean square of this directional component is equal to $1/3$ for all directions, i.e. each component of the magnetic field is isotropic, then the r.h.s. in equations (2.32) and (2.37) is equal. In other words, the magnetic field will be isotropic because it is a superposition of independent, isotropic, and uncorrelated magnetic fields, i.e. the $\boldsymbol{B}_{\boldsymbol{k}_j}(\boldsymbol{r})$.

Since the primed basis vectors are orthonormal, $\boldsymbol{\zeta}_j$ and $e^{i(k_j z'+\beta_j)}$ are independent of each other, so

$$\left\langle \left| \left[\boldsymbol{\zeta}_j e^{i(k_j z'+\beta_j)} \right]_l \right|^2 \right\rangle = \left\langle \left| [\boldsymbol{\zeta}_j]_l \right|^2 \left| e^{i(k_j z'+\beta_j)} \right|^2 \right\rangle = \left\langle \left| [\boldsymbol{\zeta}_j]_l \right|^2 \right\rangle, \tag{2.38}$$

where it is used that $\langle |e^{i(k_j z'+\beta_j)}|^2 \rangle = 1$, as $0 \leq \beta_j < 2\pi$ has no effect on the mean if $k_j|z'|_{\max} \gg 2\pi$. Requiring (2.38) to be equal to $1/3$ and using equations (2.20) and (2.22), and with notation

$\zeta_l^2 = |[\boldsymbol{\zeta}]_l|^2$ one gets for each k:

$$\langle \zeta_x^2 \rangle = \langle \sin^2(\alpha)\cos^2(\theta)\cos^2(\phi) + \sin^2(\alpha)\sin^2(\phi) \rangle = \frac{1}{3}, \tag{2.39}$$

$$\langle \zeta_y^2 \rangle = \langle \sin^2(\alpha)\cos^2(\theta)\sin^2(\phi) + \sin^2(\alpha)\cos^2(\phi) \rangle = \frac{1}{3}, \tag{2.40}$$

$$\langle \zeta_z^2 \rangle = \langle \sin^2(\alpha)\sin^2(\theta) \rangle = \frac{1}{3}. \tag{2.41}$$

Using the results from equations (2.35) and (2.36), and the constraint $0 \leq \alpha < 2\pi$ one finds that $\langle \sin^2(\alpha) \rangle = \langle \cos^2(\alpha) \rangle = 1/2$, which corresponds to a flat probability distribution $p(\alpha) = 1/2\pi$. This means that the computational algorithm may give an isotropic field. At the same time one can see that the isotropy does not depend on $\beta(k)$ or the sign in $\boldsymbol{\zeta}$. The sign (s) correspond to left- and right-circular polarisation vector , i.e. the rotation of $\mathrm{Re}(\boldsymbol{\zeta})$ around the z'-axis. If the probability distribution for the sign is not 50:50 the field will have left- or right-chirality. β is a spatial phase shift of the Fourier mode w.r.t. the origin, so in order to make the field completely random the probability distribution for β must be flat. The constraints and probability distributions of the five random parameters for isotropic fields are summarized in table 2.1.

Table 2.1: Properties of the random parameters for an isotropic field.

Parameter	Parameter range	Probability distribution
α	$0 < \alpha < 2\pi$	$p(\alpha) = 1/2\pi$
β	$0 < \beta < 2\pi$	$p(\beta) = 1/2\pi$
θ	$0 < \beta < \pi$	$p(\theta) = \sin(\theta)/2$
ϕ	$0 < \beta < 2\pi$	$p(\phi) = 1/2\pi$
s	$\{+, -\}$	$p(+) = 0.5,\ p(-) = 0.5$

In Tautz (2012) the author argues that this algorithm does not generate an isotropic field. The algorithm used is the same as described in equation (2.29), using the same rotation matrix as in equation (2.22). As the article only considers the real part of equation (2.19) as the magnetic field, the resulting B_{rms} will be halved due to the fact that the mean square value of the real part from $\boldsymbol{\zeta} e^{i(kz'+\beta)}$ is equal to that of the imaginary part. The same can be argued for the mean square value of the real part of $\boldsymbol{\zeta}$ so the requirements in equations (2.39)-(2.41) still hold for the isotropy of the field. The disagreement between Tautz (2012) and Giacalone and Jokipii (1994) arise when Tautz calculates the mean square value of $\boldsymbol{\zeta}$, where he gets the following result:

$$\langle \zeta_x^2 \rangle = \langle \sin^2(\alpha)\cos^2(\theta)\cos^2(\phi) + \sin^2(\alpha)\sin^2(\phi) \rangle = \frac{3}{8}, \tag{2.42}$$

$$\langle \zeta_y^2 \rangle = \langle \sin^2(\alpha)\cos^2(\theta)\sin^2(\phi) + \sin^2(\alpha)\cos^2(\phi) \rangle = \frac{3}{8}, \tag{2.43}$$

$$\langle \zeta_z^2 \rangle = \langle \sin^2(\alpha)\sin^2(\theta) \rangle = \frac{1}{4}. \tag{2.44}$$

Clearly $\langle |\boldsymbol{\zeta}| \rangle = 1$, but the z-component is smaller than the other two. This may be explained by assuming that Tauzt viewed the phases (α, β), and the angles (θ, ϕ) to all have a flat distribution.

If this is the case all mean square values of the sine and cosine values are 1/2, giving the result seen in equations (2.42)-(2.44). If this is the fact, then the requirement that the propagation direction of the Fourier modes has to be isotropic is violated, as it is argued in equations (2.35) and (2.36).

A visualization of this would be to use θ and ϕ as spherical coordinates on the unit sphere (which is the fact in the case of $\hat{\boldsymbol{k}}$) and distribute points on the surface of the sphere taking random values for θ and ϕ. One recognizes θ as the latitude and ϕ as the longitude. Now, if both θ and ϕ have flat probability distributions, then the points will cluster at the poles ($\theta = 0$ or π) as the longitude lines are closer together here. The distance between longitude lines is proportional to $\sin(\theta)$ and therefore the probability distribution of θ must be proportional to $\sin(\theta)$ in order to acquire equal point distribution on the unit sphere.

As mentioned in the beginning of this subsection, the article by Giacalone and Jokipii (1994) does not position the primed parameters in equation (2.19) in the same way as in this report. It is actually one cyclic permutation of the primed parameters different, with the Fourier modes propagating in x'-direction. With the same assumptions for the probability distributions of θ and ϕ as earlier in this subsection, see table 2.1, the resulting $\hat{\boldsymbol{k}}$ would not be isotropic. The case is that the article does not give probability distributions for the angles, only constraints, which leads the distributions open for interpretation. Still, the only way $\hat{\boldsymbol{k}}$ can be isotropic, given that ϕ still has a flat probability distribution, is if θ has a distribution proportional to $\cos(\theta)$ and the constraint on θ is changed to $-\pi/2 \leq \theta \leq \pi/2$. Since the constraints are given in Giacalone and Jokipii (1994), one may argue that the authors did an error, but have later realized this as in a later paper by the same authors (see Giacalone and Jokipii, 1999): There, the primed parameters are changed to match equation (2.19). The formulation of the constraints has also been improved, giving $-1 < \cos(\theta) < 1$ (Giacalone and Jokipii, 1999, p. 206) which implies a $\sin(\theta)$ distribution.

Chapter 3

Deflection

3.1 General Theory

The net force on a charged particle moving through an electromagnetic field is given by the Lorentz force law (Griffiths, 2014, p. 212):

$$\boldsymbol{F}_L = \frac{\mathrm{d}\boldsymbol{p}}{\mathrm{d}t} = q\left(\boldsymbol{E} + \boldsymbol{v} \times \boldsymbol{B}\right), \tag{3.1}$$

where $\boldsymbol{E}$ and $\boldsymbol{B}$ are respectively the electric and magnetic fields, $\boldsymbol{v}$ is the particle velocity, q is the particle charge, and $\boldsymbol{p}$ is the particle momentum. The momentum is given by the equation

$$\boldsymbol{p} = \gamma_L m \boldsymbol{v}, \tag{3.2}$$

where m is the particle mass and γ_L is the (relativistic) Lorentz factor. In the case of a zero electric field ($\boldsymbol{E} = \vec{\boldsymbol{0}}$) the acceleration of the particle due to the Lorentz force will be perpendicular to the magnetic field lines and the particle velocity. With no acceleration in the direction of the velocity, the kinetic energy of the particle is conserved. In circular motion the acceleration a is $a = v_\perp^2 / r$, where $v_\perp$ is the particle velocity and r is the radius. Using this and equation (3.1) in the case of a constant magnetic field with straight field lines the charged particles move in helical motion around the field lines with gyroradius R_g, a.k.a. the Larmor radius, given by

$$R_g = \frac{\gamma_L m v_\perp}{|q| B}. \tag{3.3}$$

The relativistic energy of a particle is $E = \gamma_L m c^2$, with c being the speed of light in vacuum. Further one may use that the charge of the particle is a sum of elementary charges e, $|q| = Ze$ where Z is an integer, so that the gyroradius may be written

$$R_g = 1.081 \cdot 10^{-3}\,\mathrm{pc} \frac{\beta_\perp}{Z} \frac{E}{10^{18}\,\mathrm{eV}} \frac{\mathrm{G}}{B}, \tag{3.4}$$

where $\beta_\perp = v_\perp / c$.

For a particle propagating through a turbulent magnetic field, one may define the gyroradius of the particle through equation (3.4) using the root mean square value of the magnetic field

strength, i.e. $B = B_{\text{rms}}$. If the gyroradius of the particle $R_g \ll L_c$, i.e. the correlation length of the field, the particle would experience the magnetic field to be approximately constant with parallel field lines on a scale size of the same order as the gyroradius. One would then expect the propagation motion of the particle to be similar to a helical motion following the magnetic field lines. In the opposite case where $R_g \gg L_c$ the magnetic field change so rapidly so that the particle would not "see" the details of the magnetic field. The particle motion would then primarily depend on the mean value of the field $\langle \boldsymbol{B} \rangle$. If the mean value is zero, one would expect the turbulence to induce small (tiny) deviations from a straight particle trajectory over scale lengths $\sim L_c$.

Caprini and Gabici (2015) give two equations for the deflection angle of electrons/positrons propagating through a turbulent magnetic field that is statistically homogeneous and isotropic. The deflection angle δ is set to depend on three parameters, namely the distance propagated D, the magnetic field's correlation length L_c and the Larmor radius, i.e. the gyroradius R_g. In the case where $D \ll L_c$ the magnetic field is approximately constant, meaning the electron/positron follow a helical motion with radius equal to the gyroradius. The deflection angle will then be

$$\delta \simeq \frac{D}{R_g} \quad \text{if} \quad D \ll L_c. \tag{3.5}$$

In the case where $D \gg L_c$ the electrons/positrons will undergo several deflections in different directions due to changes in the magnetic field. The total deflection angle in this case should be described by diffusion in angle, i.e. a random walk of small deflections, and has been calculated to be (Caprini and Gabici, 2015, p. 1; Neronov and Semikoz, 2009, p. 9)

$$\delta \simeq \frac{\sqrt{DL_c}}{R_g} \quad \text{if} \quad D \gg L_c. \tag{3.6}$$

3.1.1 Isotropic Deflection

As mentioned earlier in section 3.1 in the case of particle motion with $R_g \ll L_c$ one expects the particle motion to follow the magnetic field lines with accompanying helical motion. If the magnetic field has random isotropic turbulence, as presented in chapter 2, then the particle motion would be similar to a random walk on scale sizes much larger than L_c. The RMS value of the distance r from the origin of a random walk in 3 dimensions follow (Hemmer, 2002, p. 153)

$$\sqrt{\langle r^2 \rangle} = a\sqrt{t}, \tag{3.7}$$

where t is the time of the propagation and $a = v \cdot \mathrm{d}t$ is the length of a one step in the random walk, v is the velocity and $\mathrm{d}t$ is the time used in each step. Defining r_p as the total length propagated, one gets for the RMS distance to the origin relative to r_p

$$\sqrt{\frac{\langle r^2 \rangle}{r_p^2}} = \mathrm{d}t\sqrt{\frac{v}{r_p}}. \tag{3.8}$$

If the charged particle propagation is similar to a random walk, then at large propagation lengths the RMS of the distance to the initial position relative to the propagation length should be pro-

portional to $r_p^{-1/2}$. Note that in the opposite case $R_g \gg L_c$, i.e. small deflection angles, the RMS of the relative propagation should be close to 1, because the trajectories are approximately straight lines.

Still assuming $R_g \ll L_c$, then already at propagation lengths $\sim L_c$ the deflection angle θ_{defl} of the trajectory w.r.t. the initial propagation direction would approach that of isotropy. At these lengths the trajectories would already have preformed several helical rotations, and the field lines would have started to bend. In addition, due to the isotropy of the field and assuming the initial direction to be isotropic, the direction defined by right hand rotation of the helical motion (which is perpendicular to the initial direction) would have a flat distribution, i.e. cylindrical symmetry. The result of this is having a completely isotropic propagation direction after a propagation length $\sim L_c$, giving a probability distribution $p(\theta_{defl}) = \sin(\theta_{defl})/2$, analogous to that of θ in table 2.1. θ_{def} has then an expectation value of

$$\langle \theta_{defl} \rangle = \int_0^\pi \frac{\theta \sin(\theta)}{2} \mathrm{d}\theta = \frac{\pi}{2},$$

and standard deviation

$$\sigma_{defl} = \left(\int_0^\pi \mathrm{d}\theta \frac{\sin(\theta)}{2} \left(\theta - \frac{\pi}{2}\right)^2 \right)^{\frac{1}{2}} \approx 0.6837 \text{ rad}.$$

In the case where $R_g \geq L_c$ the propagation will not have preformed a complete helical rotation after a propagation length $\sim L_c$, but if assuming isotropic initial propagation direction, the deflection direction should still have cylindrical symmetry. For this the direction of the deflection, analogous to ϕ, is of lesser interest.

3.2 Computation Method for the Deflection Angle

After creating turbulent magnetic fields, the next goal is to compute the deflection angle of charged particle motion as a function of the propagation length in the respective fields. For this I computed particle trajectories using a Runge-Kutta (RK) solver for the equation of motion, see equations (3.1) and (3.2), which is an ordinary differential equation (ODE). The code for the Runge-Kutta solver is given in Press et al. (1997, ch. 16.2). The code has an adaptive stepsize control with error estimation in order to preform the propagation with smallest possible running time.

As argued in section 2.2.2 the computed fields would need many Fourier modes in order to be approximately isotropic, but as the computation time is proportional to the number of modes, the number of modes had to be limited. To optimize the isotropy of the fields, each field (i.e. each spectral index γ in the power law, not to be mistaken with γ_L) was computed with multiple realizations, i.e. different random parameters (see section 2.2). Then a number of particle trajectories were computed for each realization, and the results from all realizations were used to calculate the mean and RMS values.

The initial point of each particle propagation was chosen at random within a sphere with radius $\gg L_{\max}$ in order to have a random magnetic field strength, and since the Fourier modes propagate in given directions in each realization, the initial propagation direction was chosen

isotropically to ensure that the direction of a helical motion (in the case of small gyroradii, see section 3.1.1) with respect to the initial direction has isotropic distribution as well.

The particles of interest are, as mentioned in the introduction, electrons and positrons in VHE cases, i.e. $E_e \geq 1$ TeV. In these cases the speed of the particles $v \approx c$ with a relative difference less than 10^{-5}. As the Lorentz factor γ_L is highly sensitive to changes in v at these energies, it is not wise to let γ_L depend on v in the computation, as the speed may be slightly changed by the RK solver because it treats the particles classically. Therefore γ_L is rather defined by the energy $E_e = \gamma_L m_e c^2$ which theoretically is conserved during propagation in a magnetic field (see section 3.1). By checking the relative difference of the particle speed at the initial and final positions one may get an estimate on how exact the RK solver preform for the given stepsize ($\mathrm{d}r = v\,\mathrm{d}t$).

Chapter 4

Results and discussion

4.1 Normalization and Isotropy

Monte-Carlo computation was used to create all turbulent magnetic fields using the computation algorithm presented in section 2.2, where the 5 random parameters θ, ϕ, α, β and the sign $\pm$ followed the properties described in table 2.1. First one wants to examine if the fields created are normalized with a RMS value equal to the chosen B_{rms} value and with zero mean, and at what scale sizes this normalization occurs. Using MC computation to sample the field strength and direction at random positions inside a box of varying scale size centered around the origin, the mean field value $\langle \boldsymbol{B} \rangle$ and the RMS value $\langle B^2 \rangle$ could be calculated. The results from 3 random fields with spectral index $\gamma = 5/3$ (Kolmogorov turbulence) and a ratio between L_{min} and L_{max} of 0.01 can be seen in figure 4.1. As one can see from the figure the magnetic fields approach the correct normalization for the RMS value at a scale size $\sim 10\ L_{\text{max}}$. The mean field values approach zero also at a similar scale size.

From equations (2.5) and (2.26) of the normalization of the field it is clear that the ratio in the magnetic field strength between the largest and smallest scale structures are constant as long as the relative ratio between L_{min} and L_{max} is constant. This means that the magnetic field strength on scale sizes proportional to the field's scale size, e.g. L_{max}, is constant for different values of L_{max} as long as $L_{\text{min}}/L_{\text{max}}$ is constant. In other words, one may scale the magnetic field without changing its other properties. For simplicity L_{max} is therefore chosen to be 1.0. To see if the normalization change with increasing or decreasing ratio of the scale sizes or value of the spectral index, another MC computation was executed for each, both similar to that of figure 4.1. The result of both computations may be seen in figure 4.2.

From the plots in figure 4.2 it is clear that the fields approach normalization at approximately the same scale sizes, independent of the different parameters. For this reason one may be comfortable to look at the isotropy of the fields at scale sizes $\gg 10\ L_{\text{max}}$ as the fields will be normalized. In both figure 4.1 and figure 4.2 it is clear that the local field-strength varies, as one would expect for a random field. If the local field at the origin were to have another field strength, e.g. less than B_{rms}, the graphs in figures 4.1 and 4.2 would be starting at this local value.

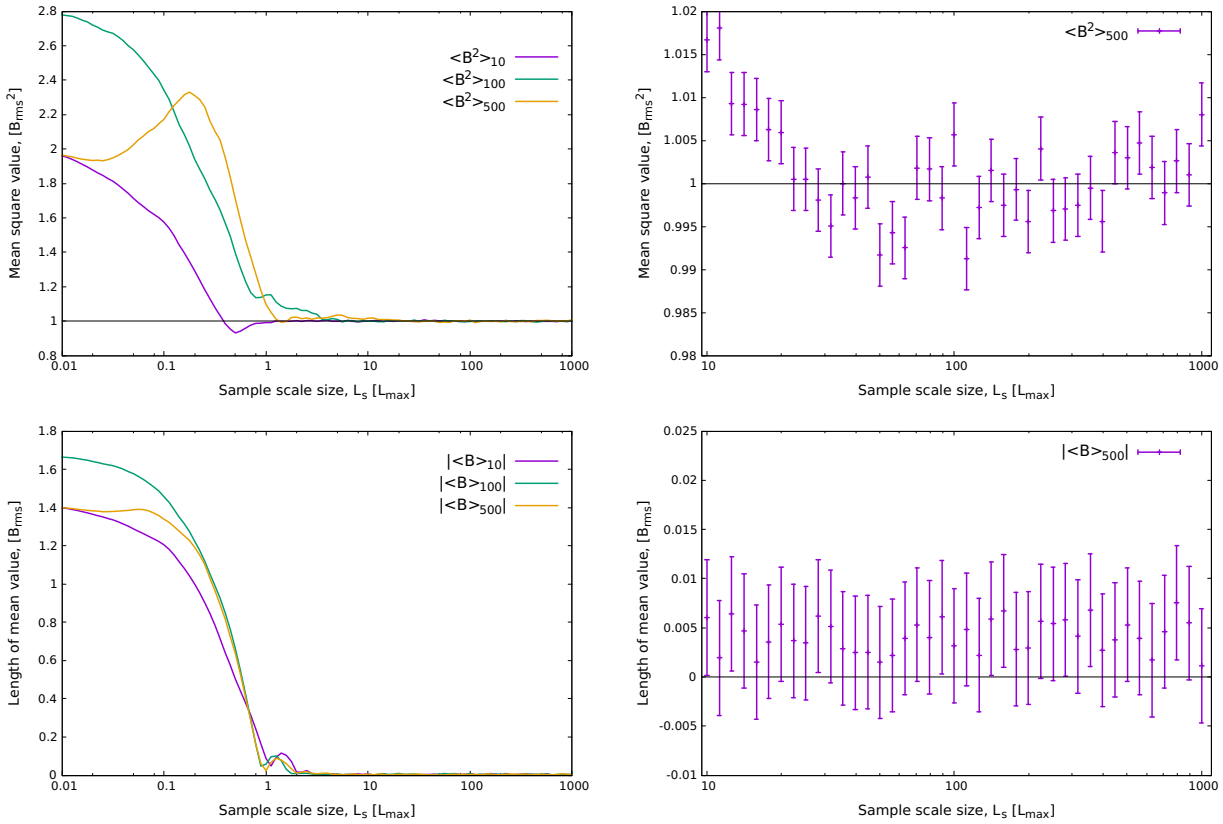

Figure 4.1: The plots show: (top) mean square values $\langle B^2 \rangle_{n_k}$, and (bottom) length of the mean $|\langle \boldsymbol{B} \rangle_{n_k}|$ of computed magnetic fields with spectral index $\gamma = 5/3$ and different number of Fourier modes n_k. Each point is a calculated mean of 50 000 samples of the magnetic field at random positions within a box of scale size L_s, with calculated standard error in the plots to the right. In all plots $L_{\max} = 1.0$, and the black lines (1.0 top, 0.0 bottom) are the expectation values for an isotropic field with zero mean and RMS value B_{rms}.

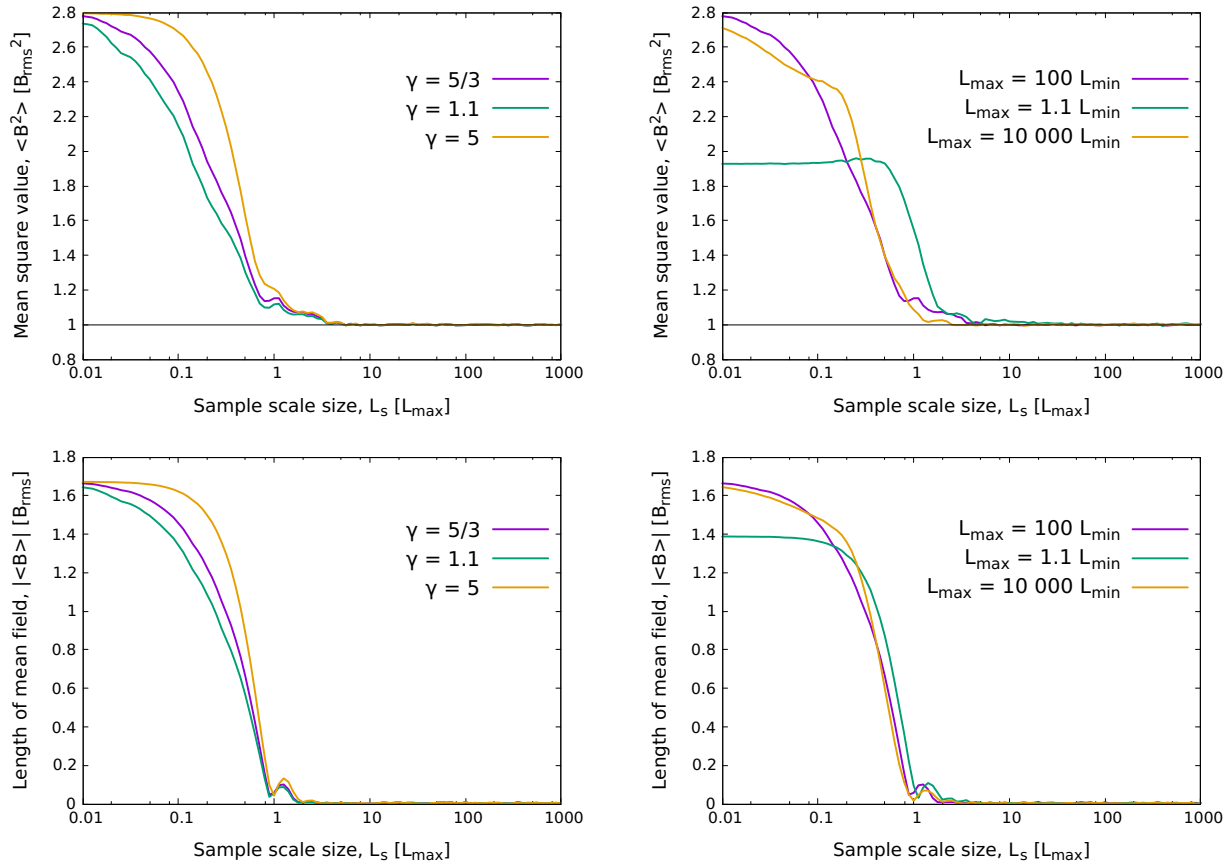

Figure 4.2: The plots show: (top) mean square values $\langle B^2 \rangle$, and (bottom) length of the mean $|\langle \boldsymbol{B} \rangle|$ of computed magnetic fields with either different spectral index γ or different ratio of $L_{\text{min}}/L_{\text{max}}$. L_{min} and L_{max} is the minimum and maximum size of the turbulent structures, and all fields are composed of 100 different Fourier modes, i.e. $n_k = 100$. Each point on the graphs is a calculated mean of 50 000 samples of the magnetic field at random positions within a box of scale size L_s, with maximum calculated standard error $\sim 10^{-2}$ B_{rms} of respective power. In all plots $L_{\text{max}} = 1.0$, and the black lines (1.0 top, 0.0 bottom) are the expectation values for an isotropic field with zero mean and RMS value B_{rms}.

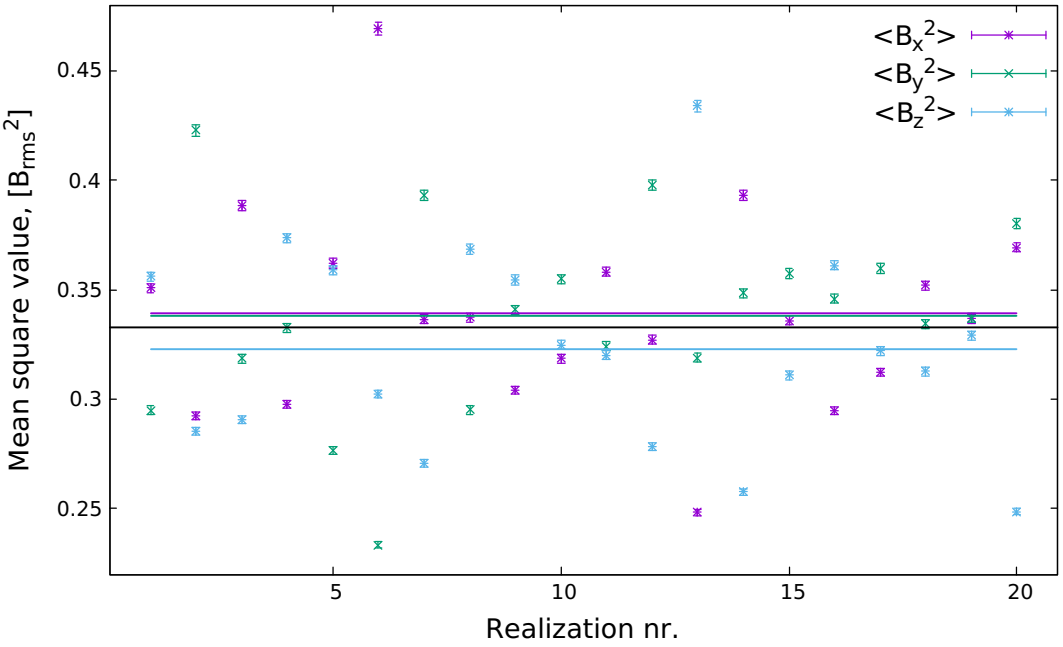

Figure 4.3: The plot shows computed mean square values of the magnetic field components for different realizations of a magnetic field with equal field parameters. Each point is a calculated mean of 50 000 samples of the magnetic field at random positions within a box of scale size $L_s = 2000\ L_{\max}$, and each mean has a calculated standard error. The colored lines are the mean values of the MS values from the different realizations, and the black line is the expected isotropic value. $\langle B_i^2 \rangle$ is the mean square value in i-direction, and the number of Fourier modes for each realization is $n_k = 100$. $L_{\max}$ is set to 1.0, $L_{\min}/L_{\max} = 0.01$, and the spectral index of the power law is $\gamma = 5/3$.

One may argue that instead of taking random positions inside a box of side length L_s one could take positions inside a sphere of the same diameter. This could arguably have been more precise to do, also in the case for isotropy as will be shown, but as one move out to the larger scale sizes $L_s \gg 10\ L_{\max}$ the field should have (approximately) zero correlation, so that a mean value inside a volume of L_s^3 will be independent of the shape. This will also be shown in the results of the spectral correlations and correlation lengths in section 4.2.

Changing the focus from normalization to isotropy, equation (2.31) requires any isotropic field to have zero mean. This is already shown to be satisfied for the magnetic fields at scale size $\gtrsim 10\ L_{\max}$, see figures 4.1 and 4.2. Having a normalized magnetic field equation (2.32) requires that the mean square value in orthonormal directions, i.e. the x-, y-, and z- components, of an isotropic field to be equal to a third of B_{rms}^2. In the first paragraph of section 2.2.2 it is argued that for a small number of Fourier modes per decade of k-values, the field will be dominated bye the few modes with small k, i.e. large scale size. Therefore to check the degree of isotropy for any field, several realizations of magnetic fields with the same parameters were computed. Each field was then sampled at 50 000 random positions inside a box of side length $L_s = 2000 L_{\max}$ to ensure normalization, and the mean square values of the x-, y-, and z-components were calculated. The result of this is shown in figure 4.3 and figure 4.4.

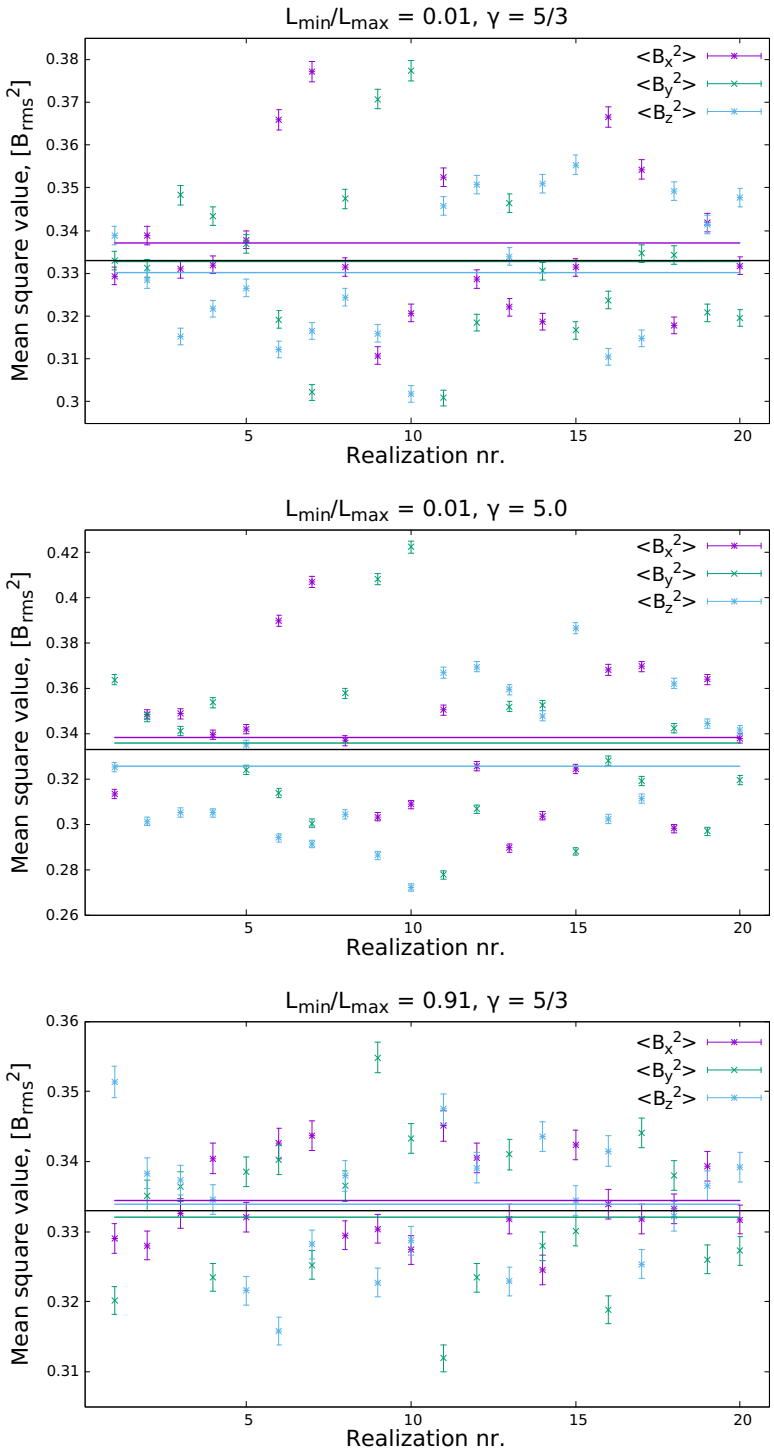

Figure 4.4: The plot shows computed mean square values of the magnetic field components for different realizations of magnetic fields with equal field parameters. Each point is a calculated mean of 50 000 samples of the magnetic field at random positions within a box of scale size $L_s = 2000\ L_{\max}$, and each mean has a calculated standard error. The colored lines are the mean values of the MS values from the different realizations, and the black line is the expected isotropic value. $\langle B_i^2 \rangle$ is the mean square value in i-direction, and the number of Fourier modes for each realization is $n_k = 100$. $L_{\min/\max}$ is the smallest/largest turbulent scale structure of the field, and γ is the spectral index.

Table 4.1: Calculated total mean with standard error of the mean square values of the field components in figure 4.3 and figure 4.4.

Number of modes n_k	Spectral index γ	Relative scale ratio $L_{\min}/L_{\max}$	Total mean of the field components in units of B^2_{rms} $\langle B_x^2\rangle_{\text{tot}}$	$\langle B_y^2\rangle_{\text{tot}}$	$\langle B_z^2\rangle_{\text{tot}}$
100	5/3	0.01	0.339 ±0.010	0.338 ±0.010	0.323 ±0.010
1000	5/3	0.01	0.3370±0.0040	0.3328±0.0044	0.3301±0.0037
1000	5/3	0.91	0.3345±0.0014	0.3321±0.0023	0.3339±0.0021
1000	5	0.01	0.3385±0.0070	0.3357±0.0082	0.3256±0.0073

Table 4.2: Calculated standard deviation of the mean square values of the field components in figure 4.3 and figure 4.4.

Number of modes n_k	Spectral index γ	Relative scale ratio $L_{\min}/L_{\max}$	Standard deviation of the field components in units of B^2_{rms} $\sqrt{\text{Var}[\langle B_x^2\rangle]}$	$\sqrt{\text{Var}[\langle B_y^2\rangle]}$	$\sqrt{\text{Var}[\langle B_z^2\rangle]}$
100	5/3	0.01	0.0465	0.0437	0.0456
1000	5/3	0.01	0.0178	0.0195	0.0164
1000	5/3	0.91	0.0062	0.0104	0.0092
1000	5	0.01	0.0312	0.0367	0.0326

In figure 4.3 one can see that for $n_k = 100$, i.e. 50 per decade of k-values, the mean square components has a substantial spread. From the plots in figure 4.4 where $n_k = 1000$ for each field, giving at least 500 modes per decade, the mean square values of the realizations have a smaller spread. This is as expected from theory as no single mode dominates a given field. Although in figure 4.4 for $\gamma = 5.0$ one gets a larger spread again as the energy spectrum becomes steeper resulting in larger ratio in power between the Fourier modes. The standard deviation and error together with the mean square values of the different realizations in the plots of figures 4.3 and 4.4 can be seen in table 4.1 and table 4.2. From the table 4.2 is is clear that the values of the standard deviations are larger than the computed mean values own error estimates in the plots in figures 4.3 and 4.4, which were $\sim 0.002\ B^2_{\text{rms}}$ in all cases.

In order to make the difference in isotropy clearer, 4 fields were realized with the same random parameters θ, ϕ, α, β and the sign $\pm$ for 100 Fourier modes. The relative scale ratio and spectral indices were changed between the realizations. Then the MS values of the field components were sampled 50 000 times at random positions, but this time inside boxes of different side lengths ranging from 500-2000 $L_{\max}$. In addition a realization with $n_k = 1000$, keeping the same parameters as for the others for the smallest k-values, i.e. the modes with most contribution to the MS. The result is seen in the plots of figure 4.5. From the figure one can see that when the spectral index γ is lowered with all other parameters constant, the field tend to become more isotropic as the MS values get closer to the expected value of 1/3. The opposite is

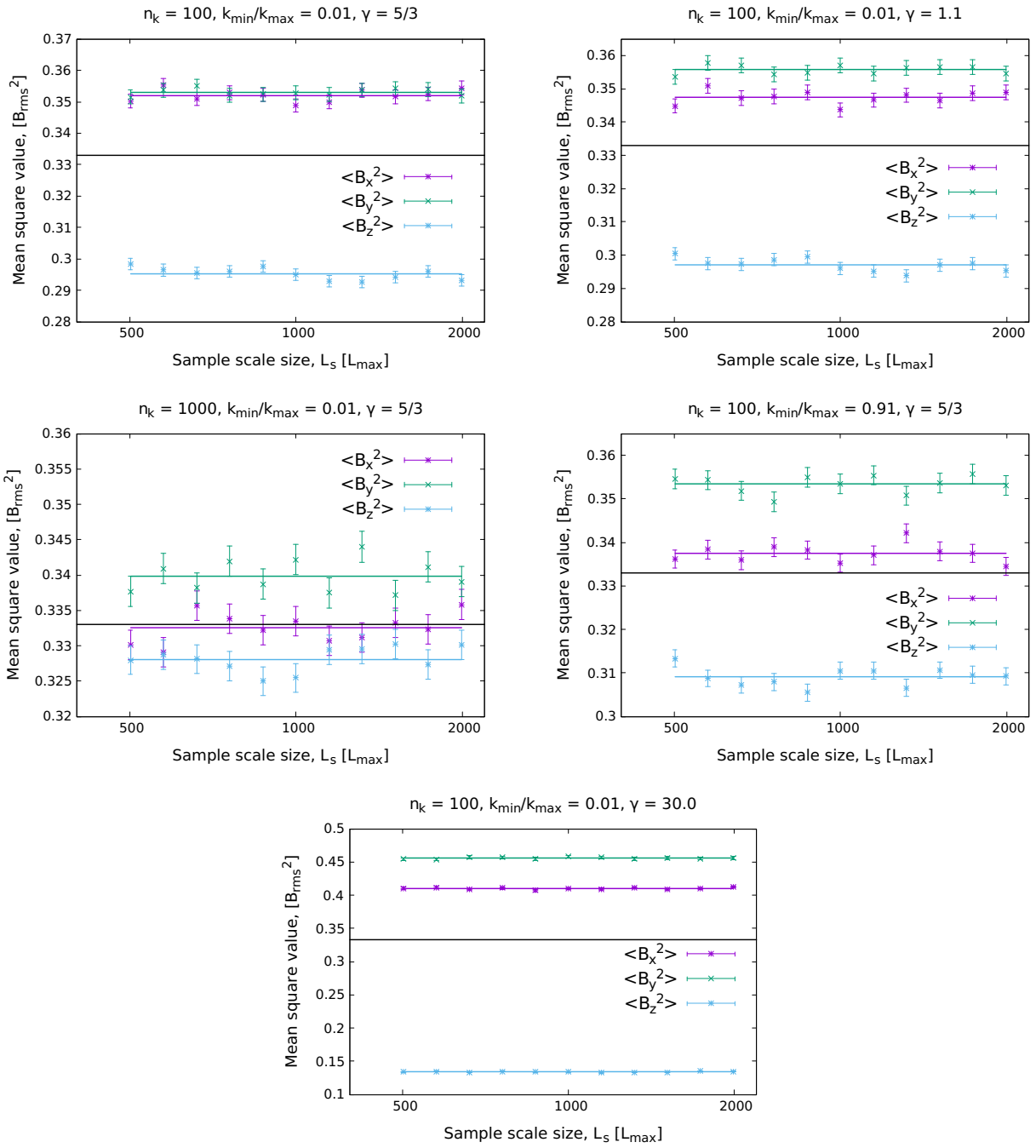

Figure 4.5: The plots show computed mean square values of the magnetic field components for computed magnetic fields with equal random numbers (see section 2.2), but different field parameters. Each point is a calculated mean of 50 000 samples of the magnetic field at random positions within a box of scale size L_s, and each mean has a calculated standard error. The colored lines are the mean values of the MS values from the different sampling scales, and the black line is the expected isotropic value. $\langle B_i^2 \rangle$ is the mean square value in i-direction, n_k is the number of Fourier modes, $k_{\min}$ and $k_{\max}$ is the minimum and maximum wavenumbers of the Fourier modes, and γ is the spectral index of the power law. In all plots $L_{\max} = 2\pi / k_{\min} = 1.0$ and $L_{\min}$ is defined by the ratio $k_{\min}/k_{\max} = L_{\min}/L_{\max}$.

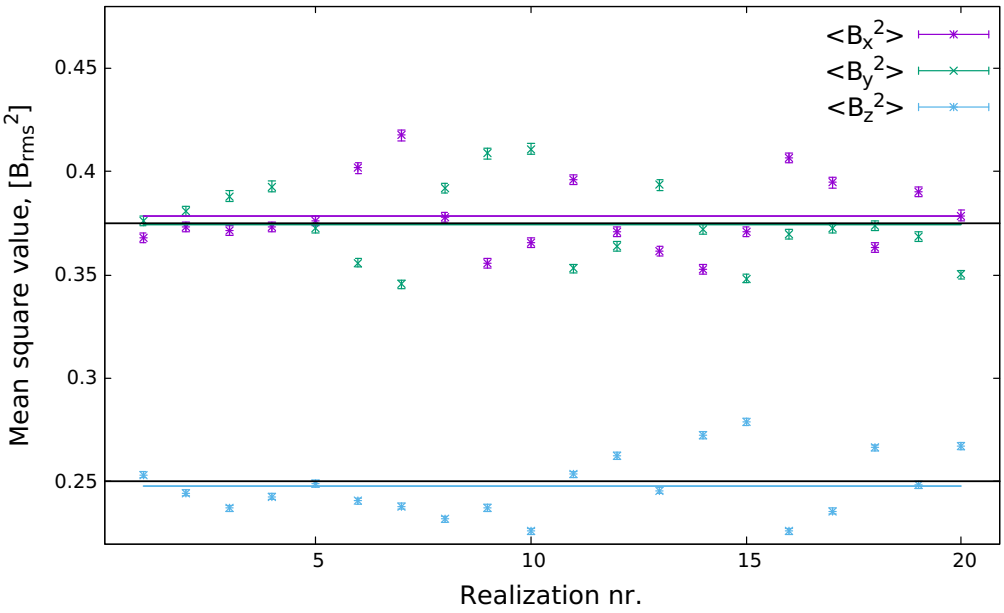

Figure 4.6: The plot shows computed mean square values of the magnetic field components for different realizations of a magnetic field with equal field parameters. The fields are computed using flat θ distribution in accordance to Tautz (2012). Each point is a calculated mean of 50 000 samples of the magnetic field at random positions within a box of scale size $L_s = 2000\ L_{\max}$, and each mean has a calculated standard error. $\langle B_i^2 \rangle$ is the mean square value in i-direction, and the number of Fourier modes for each realization is $n_k = 100$. $L_{\max}$ is set to 1.0, $L_{\min}/L_{\max} = 0.01$, and the spectral index of the power law is $\gamma = 5/3$. The colored lines are the mean values of the MS values from the different realizations, and the black lines (0.25 and 0.375) are the expected values for $\langle B_z^2 \rangle$, and $\langle B_x^2 \rangle$ and $\langle B_y^2 \rangle$ respectively.

also clear when γ is raised. Here it is set to a value of 30 so that the field is dominated by just a few modes to really show the effect. For the given values in the plot, each mode has a relative power ratio of ≈ 4 to the next mode so more than 50% lies with the smallest k-value. This in turn makes the field not isotropic. In addition, one can again see that shortening the relative ratio in scale size or increasing the total number of modes results in a more isotropic field. This is as expected from what is seen in figures 4.3 and 4.4, and because both increase the number of modes per decade of k-values.

Looking at the argument from Tautz (2012), see section 2.2.2 on page 13, the computation algorithm should not result in an isotropic field. In the mentioned section of this report, it was argued that Tautz (2012) had not successfully given θ the probability distribution required in order to make the wavevectors $\boldsymbol{k}$ isotropic. Consequently the MS value of the magnetic field components change expectation value, see equations (2.42)-(2.44). To show this θ was given a flat distribution and the MS values of the MF components was calculated in the same way as earlier, with $n_k = 1000$, $\gamma = 5/3$ and a relative turbulent scale size ratio of 0.01. The result from the computation is in accordance to the theory and is shown in figure 4.6.

To summarise the results, any computed field approach the correct normalization for the RMS of the field strength at scale sizes $\gtrsim 10 L_{\max}$, independent of γ, the $L_{\min}/L_{\max}$ ratio, and the number of Fourier modes per decade. For $\gamma = 5/3$, one needs 500 modes per decade to get a

high degree of isotropy for a computed field. The MS value of the field components are then statistically spread (≈ normal distribution) around a mean value of 1/3 B_{rms}^2, as expected for isotropy, with a standard deviation of ≈ 5% of the mean. At 50 modes per decade the standard deviation increase to ≈ 13% of the mean, meaning the fields are less likely to be isotropic. For $\gamma = 5$ the number of modes must be larger than 500 modes per decade to get the same degree of isotropy. The STD is ≈ 10% of the mean for 500 modes per decade, and further computations is needed in order to find a number of modes per decade giving STD of ≈ 5%. If the STD for $\gamma = 5$ is comparable in behaviour to that of $\gamma = 5/3$, one could approximate a STD of 3-4% for 5000 modes per decade with $\gamma = 5$. With 500 modes per decade for $\gamma = 1.1$ the STD is ≈ 2.5% of the mean, giving very isotropic fields. Finally, the disagreement of Tautz (2012) on the question of the isotropy of the computed fields was shown to be the result of wrong probability distribution of the random angle θ.

4.2 Correlation length

This part of the report aims to calculate the correlation length of the computed magnetic fields and compare them to the analytical equation (2.15) for an isotropic turbulent magnetic field with continuous k-values, following the same power law. In order to calculate the correlation lengths the following steps was done for chosen values of the spectral index γ.

1. Random fields were computed with $n_k = 100$ and 1000 for different relative turbulent scale sizes.

2. For each realization of the magnetic fields the spatial correlation function, see equation (2.17), was calculated using MC computation and length increments of

$$\mathrm{d}L = \min\left\{1/20\pi\ L_{\max},\ 1/5\ L_{c,\min}\right\},$$

   where $L_{c,\min}$ is given by the limit of equation (2.15) where the ratio of $L_{\min}/L_{\max}$ goes to zero. At each L, the spatial correlation function was calculated by sampling the magnetic field at 20 000 randomly distributed positions inside a box of side length $L_s = 1000\ L_{\max}$ and then sampling the field at one position isotropically distributed around each initial position at distance L.

3. While calculating the spatial correlation function, the correlation length was calculated in accordance with equation (2.18) by the use of Simpson's rule integration. The calculation was set to terminate if all the following was true: $L > 5L_{\max}$, the correlation length was oscillating around a seemingly constant value, and the standard deviation of the calculated L_c over the last $\Delta L = 4L_{\max}$ was smaller than the error of the Simpson's rule integration.

The results from these calculations can be seen in figures 4.7-4.9. Note that the y-axis has logarithmic spacing in all plots. There are some interesting properties of the calculated correlation lengths that one may observe in these figures.

i At larger ratios of the limiting scale sizes, $L_{\min}/L_{\max} > 0.3$, the calculated values of the correlation length follow those of the continuous field. In addition, at small values of γ ($\gamma \gtrsim 1$) this seems to be more accurate than for larger values.

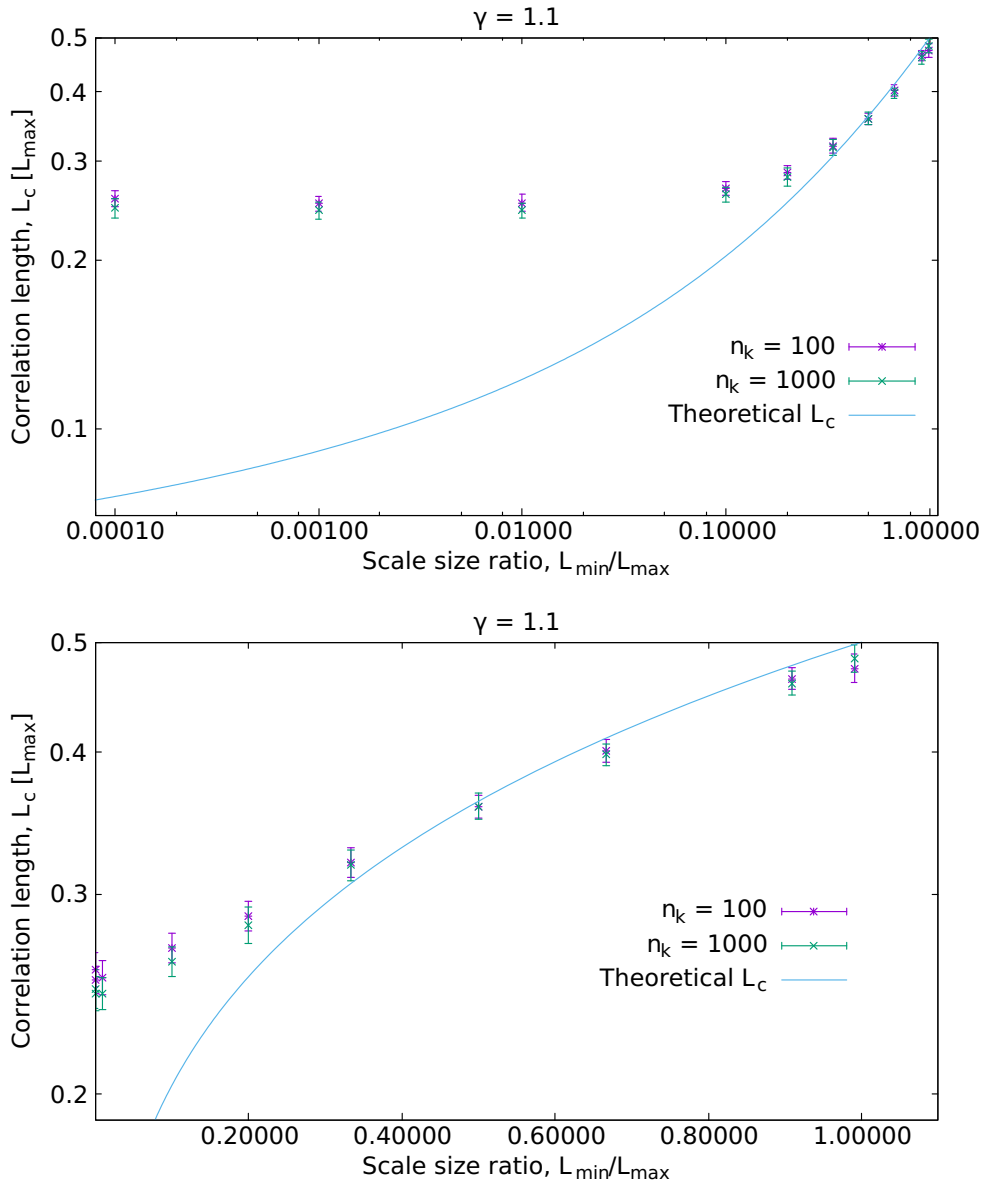

Figure 4.7: The plots show calculated correlation lengths of computed magnetic fields with spectral index $\gamma = 1.1$ and different ratios of the turbulent scale size limits. n_k is the number of Fourier modes for each field, and $L_{\max}$ is the maximum turbulent scale size. The colored line is the analytical correlation length from theory, see equation (2.15). The error of each calculated point is equal to the estimated error from the Simpson's rule integration.

ii At smaller ratios of the limiting scale sizes, $L_{\min}/L_{\max} < 0.1$, the correlation length approach a constant value different from that of the continuous field. This value also tend to be smaller for smaller values of γ.

iii A larger number of modes n_k tend to give smaller values of the correlation length.

The first observation may be explained through the combination of number of Fourier modes per decade, and the ratio in power between the modes. As the relative ratio in scale size, $L_{\min}/L_{\max}$,

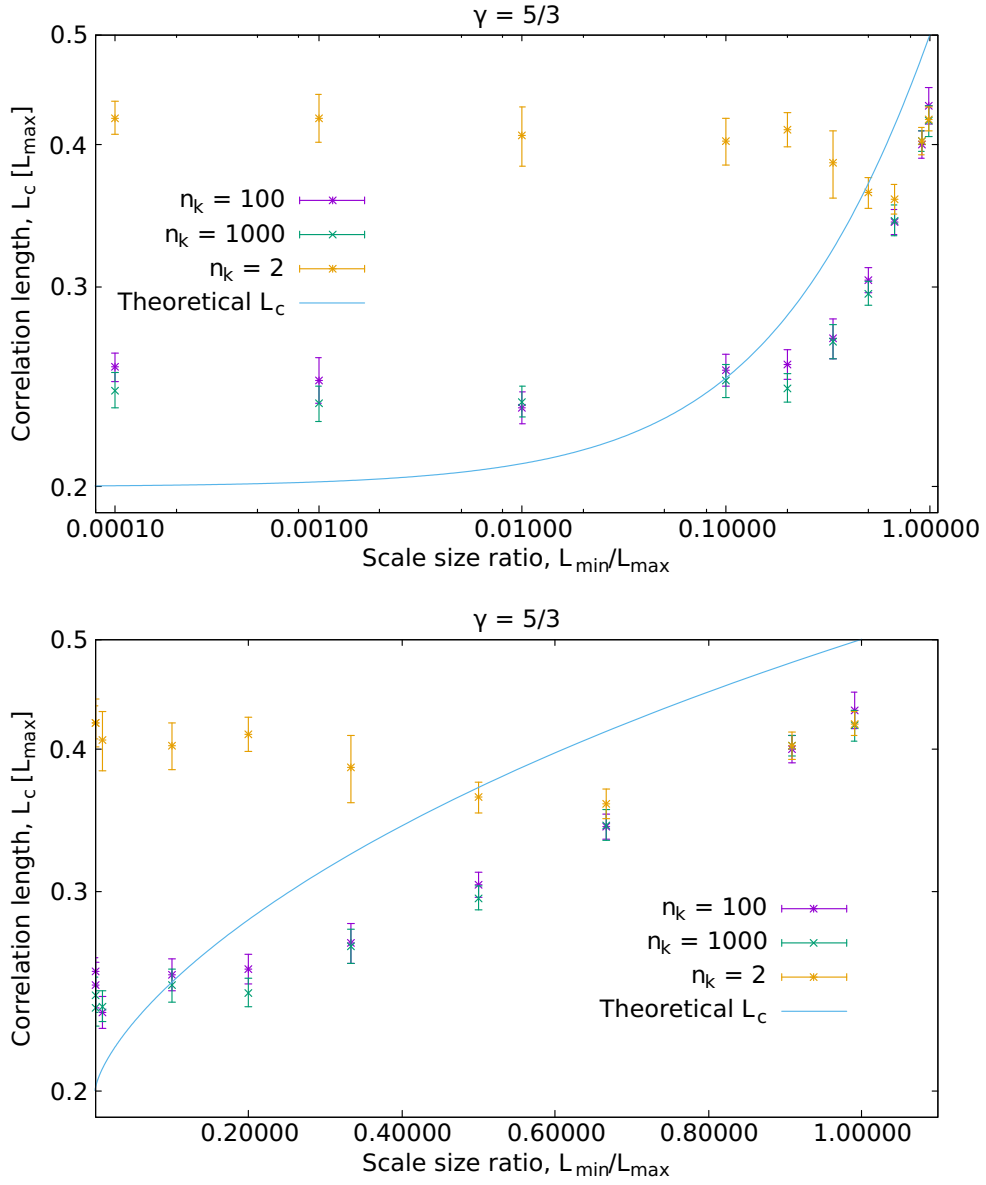

Figure 4.8: The plots show calculated correlation lengths of computed magnetic fields with spectral index $\gamma = 5/3$ and different ratios of the turbulent scale size limits. n_k is the number of Fourier modes for each field, and $L_{\max}$ is the maximum turbulent scale size. The colored line is the analytical correlation length from theory, see equation (2.15). The error of each calculated point is equal to the estimated error from the Simpson's rule integration.

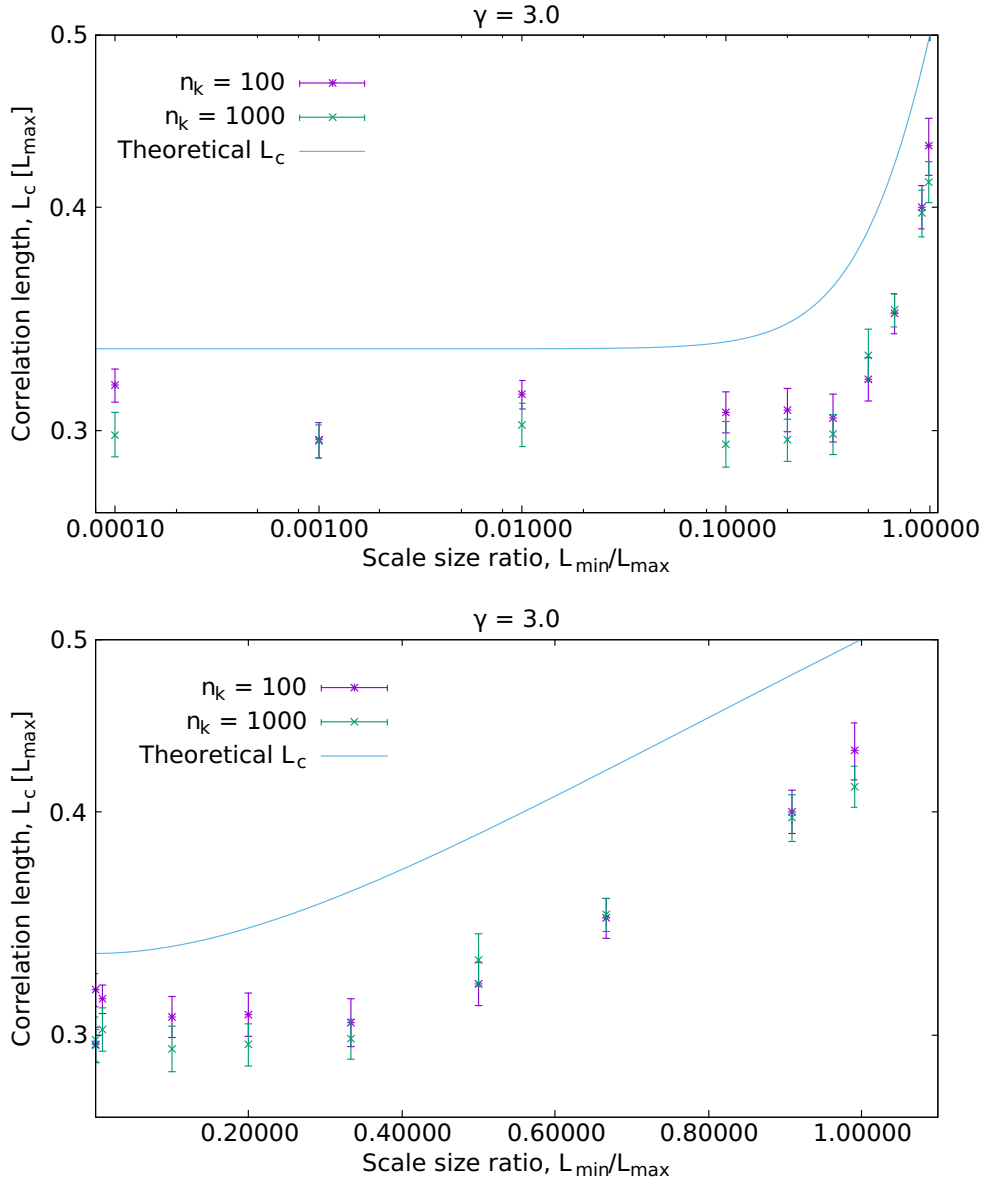

Figure 4.9: The plots show calculated correlation lengths of computed magnetic fields with spectral index $\gamma = 3.0$ and different ratios of the turbulent scale size limits. n_k is the number of Fourier modes for each field, and $L_{\max}$ is the maximum turbulent scale size. The colored line is the analytical correlation length from theory, see equation (2.15). The error of each calculated point is equal to the estimated error from the Simpson's rule integration.

is close to 1, the number of modes per decade is much larger than that of smaller ratios. At the limit $L_{\min}/L_{\max} = 1$ the field becomes constant w.r.t. k, just like the continuous field. When γ is concerned, smaller values gives power ratios of the Fourier modes close to 1, meaning more modes have a significant contribution to the magnetic field strength, which in turn makes the field more isotropic, e.g. see figures 4.4 and 4.5. As the equation for the correlation length implicitly assumes isotropy, see (2.18), the degree of isotropy of the field may influence the correlation length. In figure 4.9 one can see that at small scale size ratios L_c is not as constant for $n_k = 100$ as for $n_k = 1000$. As shown in the previous section, the computed fields are less likely to be isotropic for larger values of γ, meaning in this case that the computed fields for $n_k = 100$ and $\gamma = 3$ may not have been very isotropic, which may have led to the different L_c values at small scale size ratios. This could be an interesting objective to examine in a later project.

For the second observation, the flattening of the correlation length may be explained partly by the scale ratio. In the limit case case of observation 1 (ratio ≈ 1) all the modes change at approximately the same rate, and they also have similar strength. When the scale ratio becomes larger in the continuous case, one add more modes that change faster on spatial scales w.r.t. the largest modes. This in turn makes it so that the magnetic field change faster giving it a shorter correlation length. In the computational case one dilutes the number of modes per decade, creating fewer modes on the larger scale and more on the smaller scales. When the scale ratio becomes large the change in the number of modes per decade change less for each added decade, giving a close to constant ratio between the k-values of the modes and therefore also a constant power ratio. Increasing the scale ratio affects the magnetic field less and less resulting in a more constant correlation length.

when one is considering the spectral index and its affection on the correlation length, it is reasonable to consider the continuous case first. Since γ defines the power ration of the modes, having a larger gamma means that the added modes on lower scale sizes affect the field less than for a smaller alue of γ. In the limit where γ goes to 1, L_c goes to zero. This is explained by the fact that in this limit all turbulence scales are approximately equal in power, which in turn make the magnetic field change more on smaller scales making the spatial correlation function fall of and approach zero faster.

Looking at the difference between the analytical and computed values in the second observation one may start looking at the number of modes per decade as noted in the third observation. One can see from both figures 4.7 and 4.8 that in the case where n_k is larger the correlation length is closer to the analytical value. Two reasons may explain this. Firstly, higher density of modes (i.e. # per decade) may cause the magnetic filed to change faster as more modes have significant contributions to the field. Secondly, as for the first observation, the correlation length might be affected by the isotropy of the field. From figures 4.3 and 4.4 it is clear that a random field is more likely to be isotropic the more modes it contains. As the fields were computed with individual values it is a possibility that some of the fields had a higher degree of isotropy. For the $n_k = 1000$ fields to have the same number of modes per decade as the fields with $n_k = 100$, they would have to have a 10 times smaller scale ratio, i.e. 10 times more decades. A possible case where the consistency (or degree) of isotropy may have been the case is seen in figure 4.9 where the correlation length of the $n_k = 100$ fields are varying much more than for $n_k = 1000$ in the small scale ratio cases. Another case of this is seen in figure 4.8 where in the extreme case of $n_k = 2$, i.e. only modes for $L_{\min}$ and $L_{\max}$, when the scale ratio decreases the field is more and more defined by the $L_{\max}$ mode ($k_{\min}$). This mode is obviously not isotropic and should

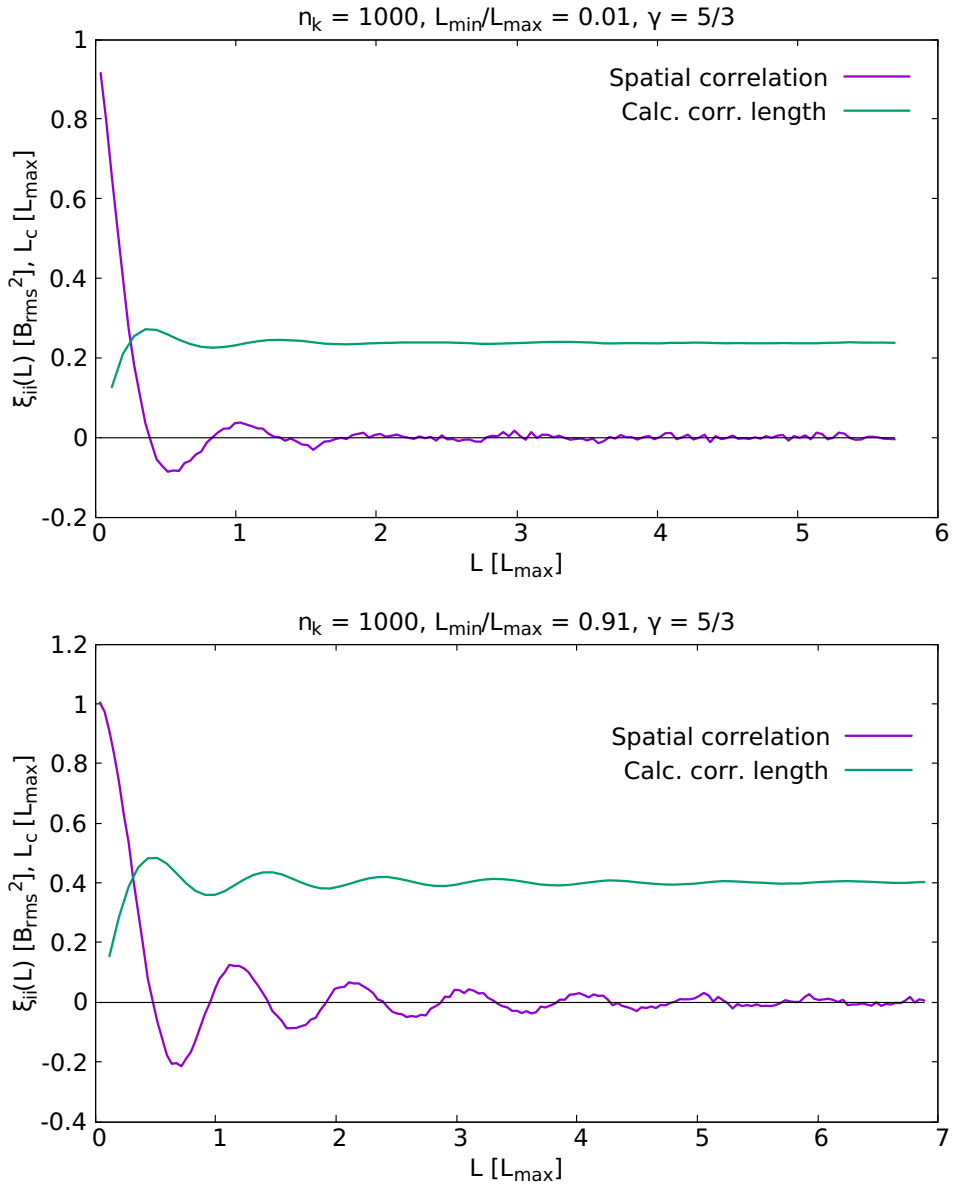

Figure 4.10: The plots show calculated spatial correlations $\xi_{ii}(L)$ as a function of distance L between two random positions in the computed magnetic fields, using the mean of 20 000 samples per L. The green graphs are the calculated correlation lengths, calculated as the cumulative result of a Simpson's rule integration of $\xi_{ii}(L)$. The field parameters are specified over each plot, with n_K = number of modes, γ = spectral index, and limiting turbulent scale sizes $L_{\min}$ and $L_{\max}$.

approach a correlation length equal to that of a single mode. This should actually be the case of all computed fields given that the number of decades surpass n_k or the spectral index become substantially large, e.g. for $\gamma = 3$ the power ratio between two modes separated by a decade is 1:1000.

What is still unclear in the case of a small scale size ratio ($L_{\min} \ll L_{\max}$) is why the calculated correlation lengths of the fields for small values of γ are larger than the analytical values, while

they for larger values of γ (see figure 4.9) suddenly become smaller?. And while this is the case observed, why is the calculated correlation lengths smaller for larger n_k in all cases of γ? The latter has been discussed in the two previous paragraphs, but any distinct answer to this question has not yet been given, nor will be in this report. The first question is not easily answered as well. At this moment one could turn to the computation method for the correlation length. The method given earlier in this section do contain statistical and possibly also systematic errors. The statistical error in the MC sampling of the correlation length and the length increment dL may have had a significant effect of the result of the Simpson's rule integration.

Two examples of the calculated spatial correlation function with accumulated Simpson's rule integration for L_c may be seen in figure 4.10. It is worth noting that a decrease in dL, i.e. more sample points per length, without increasing the number of positions sampled in each MC sampling could contribute to a higher estimated error of the integration. From the plots one can also see that the spatial correlation function is not smooth due to the statistical error (i.e. standard error of the mean) of the MC sampling. One would be motivated to try and decrease this error, but in order to decrease the error by a factor of 2 one would increase the number of samples and therefor also the computation time by a factor of 4. With the computational power disposable, this was the limiting factor. For later studies either having more time or more computer power would open for an increase of MC samples.

Let's summarise the results in this section: For relative scale ratios $L_{\min}/L_{\max} > 0.5$ and spectral indices close to 1 the correlation length of the computed fields follow the analytical correlation length of a continuous field with continuous modes and equal power spectrum. In the limit $L_{\min}/L_{\max} = 1$ the correlation length of the computed fields goes towards $0.5L_{\max}$. At small scales size ratios $L_{\min}/L_{\max} \ll 1$ the correlation length approaches a constant value in the range 0.0-0.5$L_{\max}$. This value is in general different from that which is expected from the continuous field. The constant value is larger for larger values of γ, but seams to decrease with an increasing number of modes per decade. Whether the degree of isotropy of the computed fields affect the correlation length is not explicitly shown, but there are indications that higher degree of isotropy give more stable correlation lengths. For all values of γ, the differences in calculated correlation lengths are small between fields with a total number of modes of 100 and 1000.

4.3 Deflection Angle

This part of the report aims to calculate the deflection angle of VHE electrons/positrons propagating through turbulent magnetic fields and then compare the results to the analytical expectations presented in section 3.1. To calculate the deflection angles, the method presented in section 3.2 was used with the following parameters for the fields: RMS value of the field strength, $B_{\text{rms}} = 10^{-6}$ G, the number of Fourier modes per field, $n_k = 100$, and the maximum scale size $L_{\max} = 1$ pc. The reason for choosing $n_k = 100$, although it gives fields with not so high degree of isotropy, is the computational time it demands. With more time or computational power, this number could have been increased. To compensate for the isotropy each field was created with a certain number of field realizations, $N_r = 25$. The number of particle trajectories per field realization was set to $N_p = 50$. The chosen scale size ratios and spectral indices for the fields can be seen in table 4.3, with accompanying correlation lengths from the results in section 4.2. From equation (3.4) one would with electron energy $E_e = 1$ TeV get a gyroradius $R_g = 1.081 \cdot 10^{-3}$ pc,

Table 4.3: Field parameters with calculated correlation length for computed turbulent magnetic fields with 100 Fourier modes.

Relative scale ratio L_{min}/L_{max}	Spectral index γ	Correlation length L_c [L_{max}]
0.01	5/3	0.23
0.01	3.0	0.31
0.01	1.1	0.25
0.91	5/3	0.40
0.91	3.0	0.40
0.91	1.1	0.46

which would be of order 10^{-2} smaller than the correlation length of any of the computed fields.

The electron energies was chosen so that the gyroradius the electrons ranged from $10^{-2} - 10^5\ L_c$, calculated using equation (3.4) with insertion of $B = B_{rms}$. Then the particle trajectories were computed and all the distances propagated, positions and velocities were tracked. At certain propagation lengths the deflection angle was calculated and the results can be seen in figure 4.11 to figure 4.18. Note: For the computations of the particle trajectories the time increment of the Runge-Kutta solver was set so that the propagation between 2 tracking-positions was equal to or less than $L_c/300$ for trajectories less than 10 L_c in length. This is so that the particles with smaller gyroradius should not be able to complete a greater part of a circle motion between the tracking. It should simultaneously be noted that the RK-solver compute several steps between the two tracking-positions. In the computed trajectories with propagation distance $> 10L_c$ only electrons with gyroradius of order $10^3\ L_c$ and higher was considered. Due to very small deflections the time increment of the RK-solver was then set so that the distance increments was approximately $L_c/2$. This was in order to decrease the computation time, else it would run for many days. As mentioned in section 3.2 it is important that the change in particle speed due to the RK-solver are negligible. In the case for the lowest energies (where $D = (0.01 - 10)L_c$) the largest relative change of the particle speed in any propagation was of order 10^{-6}, while for the higher energies ($D > 10L_c$) the largest relative change was of order 10^{-7}. This indicates that the time increment for the RK-sovler was sufficient in order to secure valid results as the speed and energy is considered to be constant.

The choice of units is made to simplify equations (3.5) and (3.6), and to make the plots in the figures (see 4.13-4.18) more comparable to each other. At small propagation lengths $D < 0.1L_c$ in all of the mentioned figures the mean deflection angle follow the analytical expectation value from equation (3.5) independent of γ or particle energy (i.e. gyroradius). In the case of the smallest energies, see figures 4.13 and 4.15, the gyroradii are of the same order or less than the propagation length. This would in general result in deflection angles larger than π as helical motion would occur. As the deflection angle in the computation is calculated using the initial and current velocity, any angle larger than π will be lost. In the cases where the propagation length $D \gg R_g$ the distribution of velocity directions should approach an isotropic distribution, giving a mean value of $\pi/2$ with a standard deviation of 0.6837, see section 3.1.1. This is best

shown in figure 4.11 where the mean deflection angle for electrons with gyroradii $R_g = 0.01$ and $0.1\ R_g = L_c$ is plotted together with the calculated standard deviation. One can see that for both energies the deflection angle approaches isotropy at a propagation distance of $2L_c$.

In figure 4.12 the case with small gyroradii is further examined. The figure shows a plot of the RMS value of the distance from the initial point relative to the propagation length. The black line in the plot represent a function following a random walk distribution following $AD^{-1/2}$, A being a constant (see equation (3.8)), but with a different value of A than what would be expected from the computation parameters. The line is there to observe the asymptotic behavior of the RMS value. One see that for $D < 2L_c$ the RMS value seems approach the same asymptotic behaviour, but two sample points are too few to be able to draw any conclusions. A new computation would have to be preformed, but not be done in this report. Not because it is unimportant, but the computation time this would require is too great.

Looking at the bottom plots in figures 4.13 and 4.15, where the gyroradius of the electrons are of order $1 - 10\,L_c$, one can see that in the case of short propagation lengths equation (3.5) is fulfilled. While equation (3.6) would expect the deflection angles at longer propagation lengths $D \gg L_c$ to be proportional to $\sqrt{D}/R_g$, the mean deflection angles (especially for $R_g = 1L_c$) approach $\pi/2$ before this large scale limit. As argued before, the computational algorithm loose all values of the deflection angle larger than π, and the expectation value for the deflection angle is $\pi/2$ even if the true deflection is $\gg \pi$. Using what is seen for $R_g = 0.1L_c$ one would expect that the mean deflection angle for both $R_g = 1Lc$ and $R_g = 10L_c$ would reach and stabilize around $\pi/2$ for propagation lengths $D \gg L_c$ and not follow the analytical value of equation (3.6). Unfortunately the plots terminate at $D = 10L_c$ where $\langle\delta\rangle \approx \pi/2$ for $R_g = 1L_c$. In order to check the expectations one would have to increase the propagation length of the computed particle trajectories, which as mentioned before would also increase computation time.

Now starting too look at the weak field case, i.e. $R_g \gg L_c$. As mentioned earlier, equation (3.5) holds at short propagation distances (e.g. see figure 4.14). When one moves out to larger propagation distances one sees that the calculated deflection angles start to deviate from the analytical values, see figures 4.14, 4.16 and 4.18. Taking now a closer look at the boundary points between the two computations in each plot. By this we mean the calculated deflection angles for the same electron energies, but for the different computations where the time increment of the RK-solver was different. One can see that generally for all energies the calculated deflection angles coming from the smaller propagation distances seem to make a smooth curve in the transition between $D < 0.1L_c$ to $D > 10L_c$. Also, these deflection angles seem to approach the analytical equation, see (3.6), at their right limit.

When looking at the deflection angles calculated in the second computation, one can see that many of the values deviate from the first computation where they overlap, e.g. see figure 4.16. In addition there are big outliers that make little sense, again see figure 4.16. These deviations may indicate some errors in the computational code, but as it didn't give strange results for the other γ values this would be strange. As the deflection angles don't overlap, one should be cautious to draw any conclusions from the results. A possible answer to the deviations may lie in the value of γ. As γ define the power ratio of the scale sizes, with a smaller γ giving more power to the smaller scales, it might happen that the chosen time increment for the RK-solver is too large. One should note that decreasing the time increment lead to longer computation time. Additional computations with new fields may also show if these outliers in the plots are coincidences or not, but as the other plots indicate they would probably follow the same deviation

from the analytical values.

In figure 4.18 the computation is run with a relative scale size difference of 0.91 as opposed to 0.01 in the other figures. Here one continues to see deviations from the analytical values, but here the calculated values for $\gamma = 1.1$ follow the same behaviour as for $\gamma = 5/3$ without the outliers one can see in figure 4.16. This strengthens the already established suspicion that there could be something wrong with the results in figure 4.16.

The time increment was mentioned as a possible explanation to the deviations seen in figure 4.16, but what if this is the cause of the deviations in all of figures 4.14, 4.16 and 4.18? This could be a possibility, but checking this with additional computations with much smaller time increments would take days of computation time and is not manageable with the limited time left of this project. Computation time will always be a limiting factor in this form of research, so compromises must sometimes be made and precision be sacrificed for efficiency.

After analyzing the figures and observing that all deflection angles at longer propagation lengths deviate from the analytical formula in the same way, there is one property of the field that must be considered, namely the correlation length. As equation (3.6) depend on the field's correlation length while equation (3.5) do not, only the analytical deflection angles at long propagation lengths is affected by a change in L_c. It's important to remember that equation (3.6) requires $D \gg L_c$, while equation (3.5) requires $D \ll L_c$. The correlation lengths used for the deflection angle calculation were those calculated in section 4.2. These correlation lengths did have calculated errors, but it is worth noticing that each one was calculated using only 1 realization of each field, which may therefore not be representative of a set of several realizations. Let's look at the correlation length required for the calculated means of the deflection angles for the electrons with the largest gyroradius ($R_g = 10^5 L_c$) to match the analytical values. The reason for this choice is that these gyroradii seem to be behaving equally w.r.t. the analytical expectation for $\gamma = 5/3$ and $\gamma = 3$. Figure 4.14 gives $\langle\delta\rangle = (9.54 \pm 0.77) \cdot 10^{-5}$ at $D = 1000 \cdot 0.23 L_{\max}$ for $\gamma = 5/3$ and $R_g = 0.31 \cdot 10^5 L_{\max}$. This corresponds to $L_c = (0.021 \pm 0.003) L_{\max}$ in equation (3.6). Note that table 4.3 had to be used in order to transform D and R_g into scalars of $L_{\max}$. Figure 4.17 gives $\langle\delta\rangle = (1.09 \pm 0.10) \cdot 10^{-4}$ at $D = 1000 \cdot 0.31 L_{\max}$ for $\gamma = 5/3$ and $R_g = 0.31 \cdot 10^5 L_{\max}$. This corresponds to $L_c = (0.036 \pm 0.007) L_{\max}$. One see clearly that both correlation lengths needed to equate the analytical equation to the results are of order 10^{-1} w.r.t. those calculated in section 4.2 and are way outside the error estimates. For this the correlation lengths do not seem to be the source to the deflection angle deviations.

In addition to the proposed sources for error there is one more that should be mentioned. As shown in section 4.1, if using only $n_k = 100$ Fourier modes when the relative turbulent scale size ratio was 0.01, i.e. 50 modes per decade, the computed fields are in a few cases not very isotropic. This potential deviation from isotropy may have contributed to the deviations seen in the deflection angles at longer propagation lengths, but without further testing this can not be confirmed. An attempt to try to counteract the possible deviations from isotropy has been made by using multiple realizations of the fields when computing the particle trajectories, which should give a more isotropic filed on average and therefore possibly improve the result (see figure 4.3. In section 4.1 it was also argued that decreasing the number of decades, i.e. setting $L_{\min}$ closer to the value of $L_{\max}$, will improve a computed field's isotropy. Although turbulent field where $L_{\min} \lesssim L_{\max}$ may not be very physical, we are looking at theoretical fields in this report. Looking again to figure 4.18 where the relative scale ratio is 0.91 and comparing the results to those for the same values of γ for a relative scale ratio of 0.01 (see figures 4.14 and 4.16) one

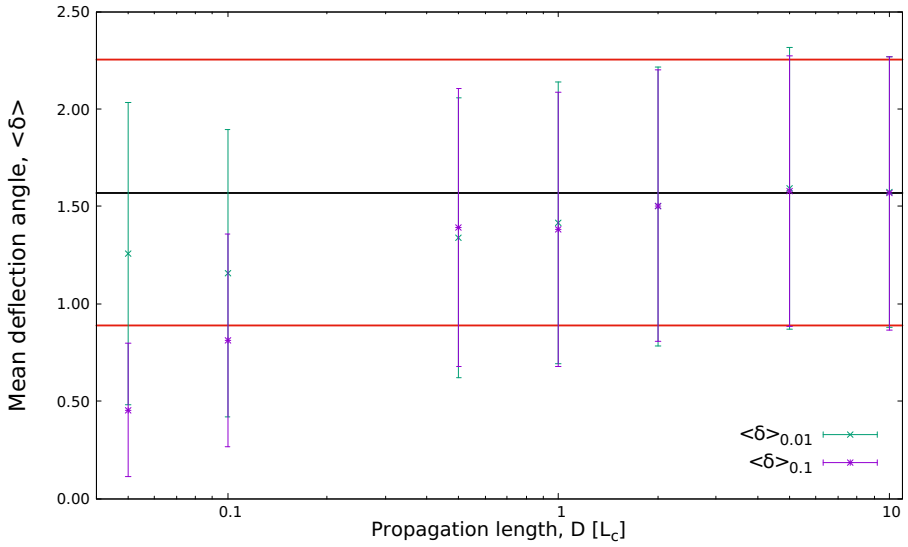

Figure 4.11: The plot shows calculated deflection angles for electrons/positrons propagating through computed magnetic fields with spectral index $\gamma = 5/3$, relative turbulence scale size ratio $L_{\min}/L_{\max} = 0.01$, number of Fourier modes $n_k = 100$, and correlation length $L_c = 0.23$. $\langle\delta\rangle_x$ is the mean deflection angle for the electrons/positrons with gyroradius $R_g = x \cdot L_c$. The bars represent the standard deviation of the set of deflection angles used to calculate each mean. The black line represent a deflection angle of $\pi/2$ and the red lines have values equal to $\pi/2 \pm 0.6837$, representing the analytical standard deviation of the deflection angle at isotropic distribution.

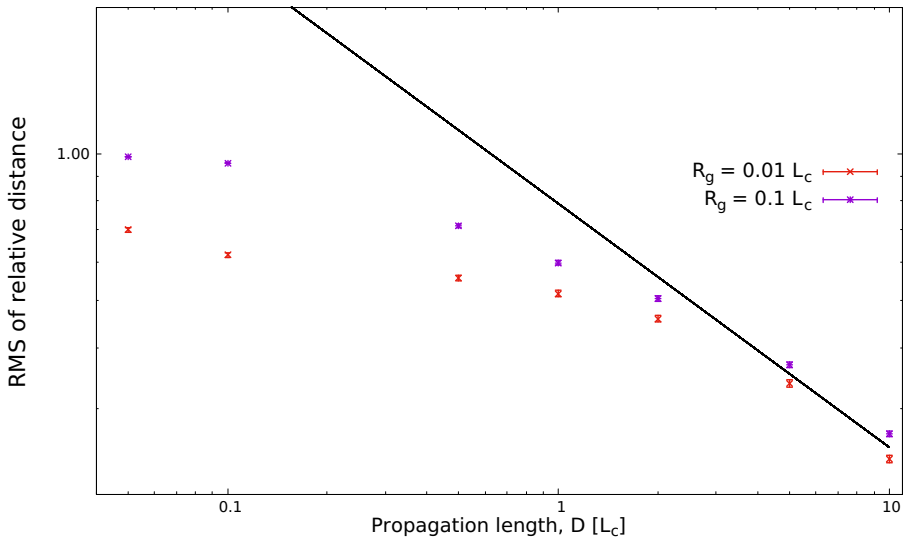

Figure 4.12: The plot shows the calculated RMS values of the distance from the origin relative to the distance propagated D for electrons/positrons propagating through computed magnetic fields with spectral index $\gamma = 5/3$, relative turbulence scale size ratio $L_{\min}/L_{\max} = 0.01$, number of Fourier modes $n_k = 100$, and correlation length $L_c = 0.23$. The black line represent a function proportional to $D^{-1/2}$.

sees little to no difference between the results. This is especially the case for $\gamma = 5/3$, which is the value most studied in this report. To examine if isotropy, or the lack of it, actually do contribute to the deviation seen, additional computations must be made. Possible changes could be increasing (or decreasing) the total number of Fourier modes n_k or increasing the number of realizations of each field. In the end there is always the probability that the analytical equation does not correctly describe the deflection angles of particles moving through the computed fields, but without any further tests this is impossible to prove.

A final possibility is that the deviation from the analytical formula is real. A confirmation of this claim would require an extreme amount of testing, double checking all parts of the computational code, and a thorough analysis of any possible source of error. Considering the time limit for this projects, an answer to this statement is far beyond the reach of this report.

To summarise this section we have seen that the mean deflection angles of electrons propagating through the computed magnetic fields follow the analytical formula for propagation lengths $D \ll L_c$, see equation (3.5). On the contrary one sees that at longer propagation lengths $D \gg L_c$ the mean deflection angles deviate from the analytical expectations, see equation (3.6). In order for the deflection angles to match the expected values, the correlation lengths would have to be 10 times smaller than what was calculated in section 4.2. In addition at propagation lengths $D > R_g$ the mean deflection angle approaches $\pi/2$ as the velocity directions approach isotropic distribution, due to the fact that the computational algorithm loses track of angles $\delta > \pi$. The most probable sources of error when trying to explain the deviations in deflection angles relative the analytical expectations are the time increment of the Runge-Kutta solver in the computational algorithm, and the computed fields isotropy. Both potential sources require additional testing with smaller time increments and more Fourier modes, which requires more time than what is possible within the time window of this project.

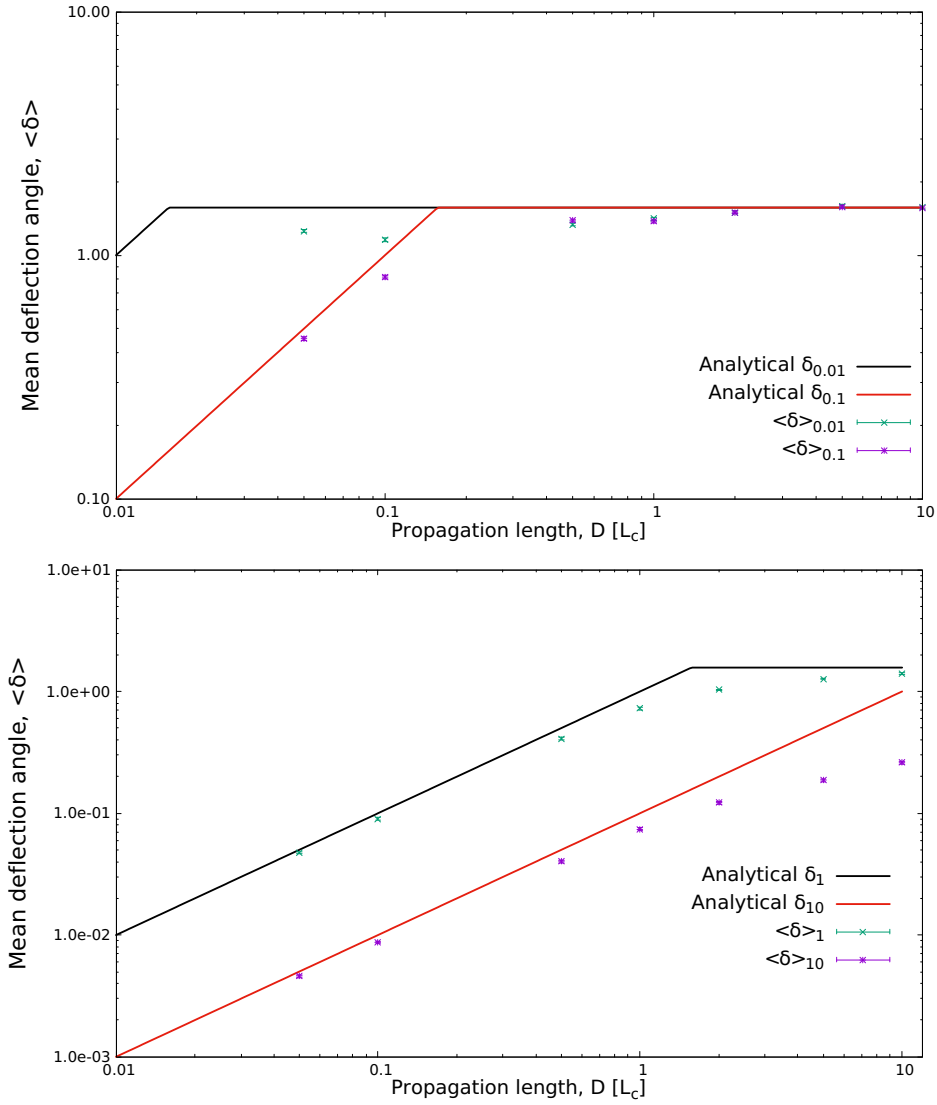

Figure 4.13: The plots show calculated deflection angles for electrons/positrons propagating through computed magnetic fields with spectral index $\gamma = 5/3$, relative turbulence scale size ratio $L_{\min}/L_{\max} = 0.01$, number of Fourier modes $n_k = 100$, and correlation length $L_c = 0.23$. $\langle\delta\rangle_x$ is the mean deflection angle for the electrons/positrons with gyroradius $R_g = x \cdot L_c$. The bars represent the standard error of the mean and the solid lines are the analytical expectation values in the limits of the propagation length $D \ll L_c$ (see equations (3.5)). Where the analytical values reach $\pi/2$ they are set to be constant.

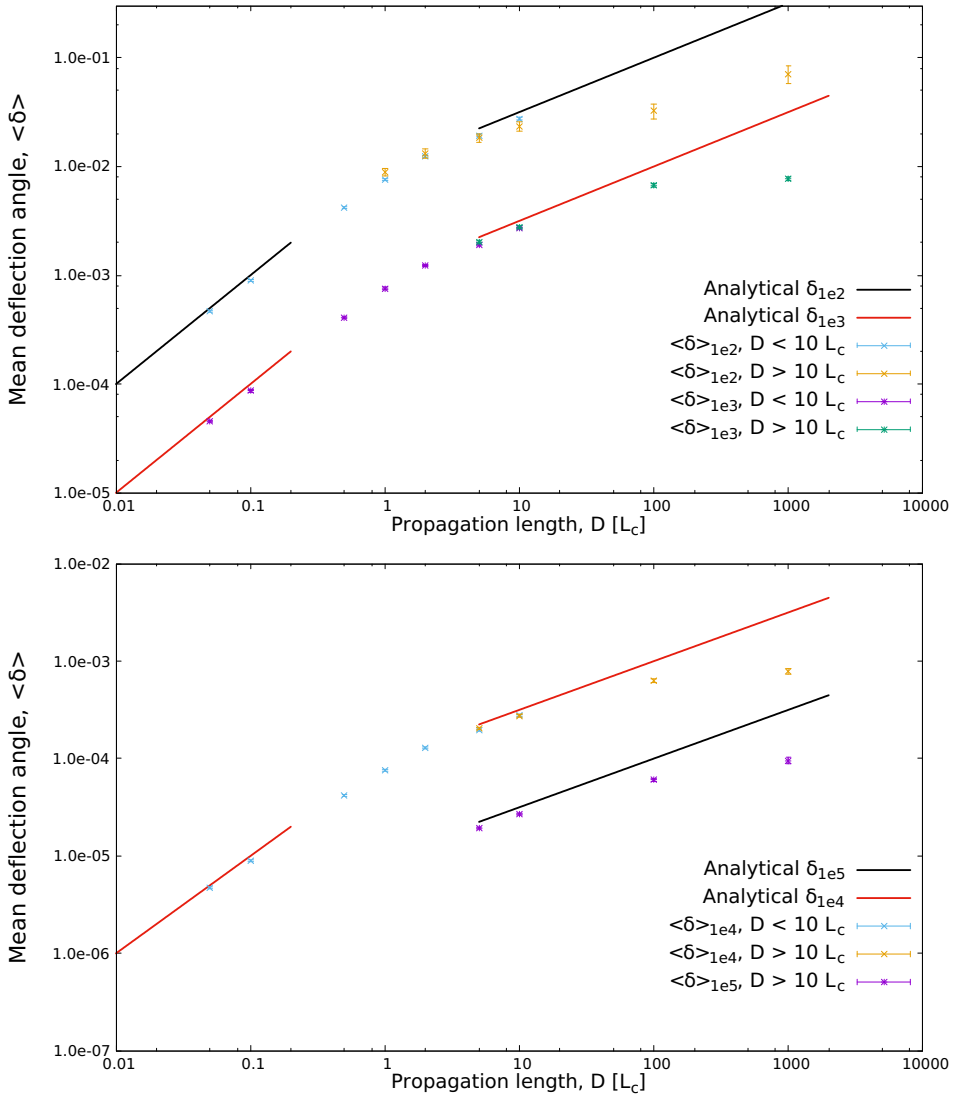

Figure 4.14: The plots show calculated deflection angles for electrons/positrons propagating through computed magnetic fields with spectral index $\gamma = 5/3$, relative turbulence scale size ratio $L_{\min}/L_{\max} = 0.01$, number of Fourier modes $n_k = 100$, and correlation length $L_c = 0.23$. $\langle\delta\rangle_x$ is the mean deflection angle for the electrons/positrons with gyroradius $R_g = x \cdot L_c$. The bars represent the standard error of the mean and the solid lines are the analytical expectation values in the limits of the propagation length $D \ll L_c$ and $D \gg L_c$ (see equations (3.5) and (3.6)).

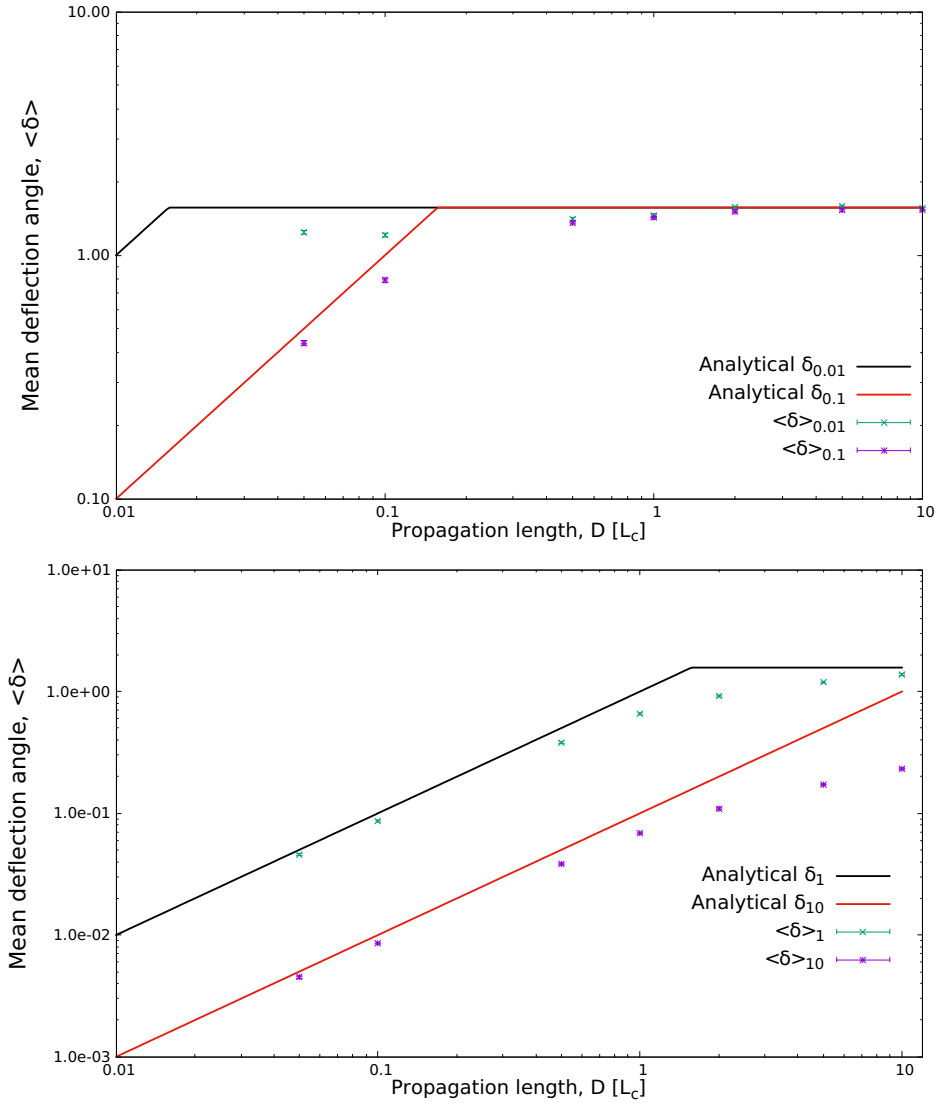

Figure 4.15: The plots show calculated deflection angles for electrons/positrons propagating through computed magnetic fields with spectral index $\gamma = 1.1$, relative turbulence scale size ratio $L_{\min}/L_{\max} = 0.01$, number of Fourier modes $n_k = 100$, and correlation length $L_c = 0.25$. $\langle\delta\rangle_x$ is the mean deflection angle for the electrons/positrons with gyroradius $R_g = x \cdot L_c$. The bars represent the standard error of the mean and the solid lines are the analytical expectation values in the limits of the propagation length $D \ll L_c$ (see equations (3.5)). Where the analytical values reach $\pi/2$ they are set to be constant.

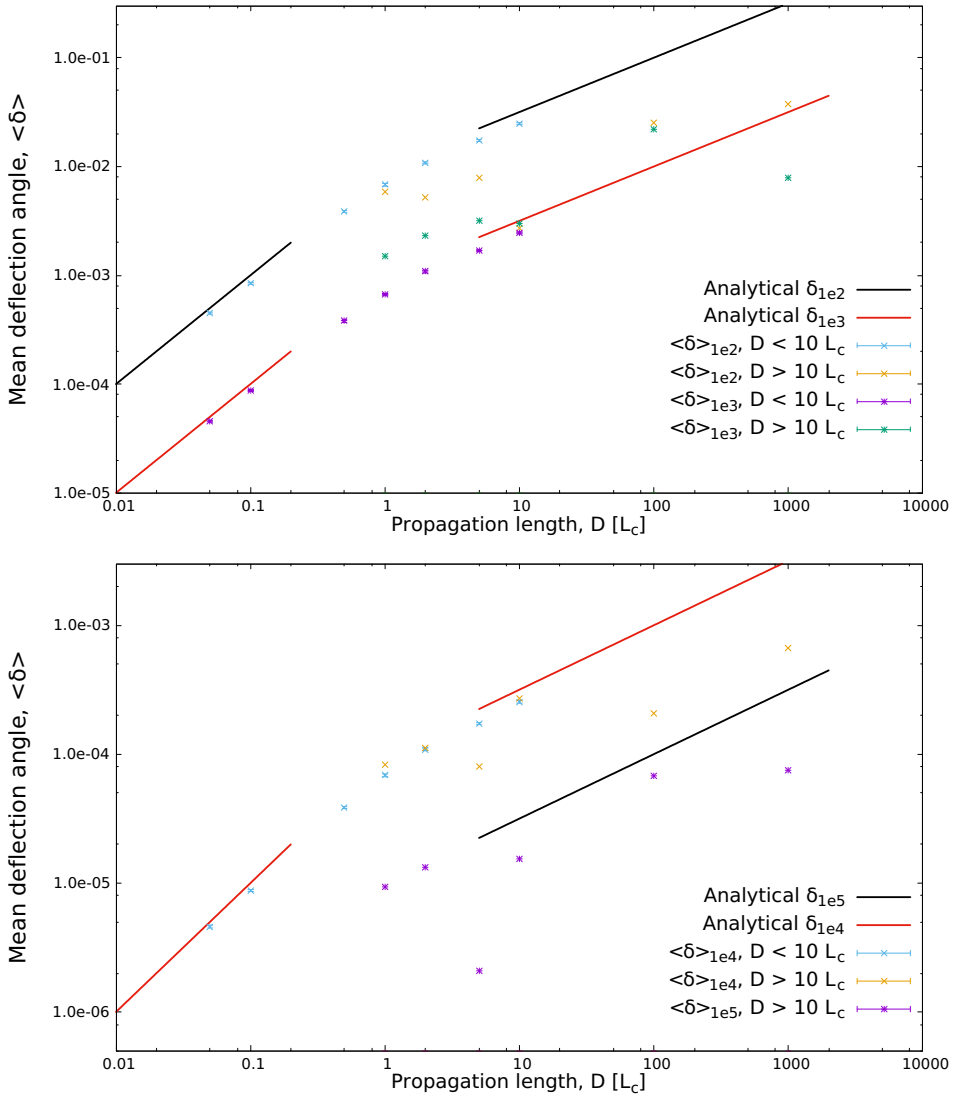

Figure 4.16: The plots show calculated deflection angles for electrons/positrons propagating through computed magnetic fields with spectral index $\gamma = 1.1$, relative turbulence scale size ratio $L_{\min}/L_{\max} = 0.01$, number of Fourier modes $n_k = 100$, and correlation length $L_c = 0.25$. $\langle\delta\rangle_x$ is the mean deflection angle for the electrons/positrons with gyroradius $R_g = x \cdot L_c$. The bars represent the standard error of the mean and the solid lines are the analytical expectation values in the limits of the propagation length $D \ll L_c$ and $D \gg L_c$ (see equations (3.5) and (3.6)).

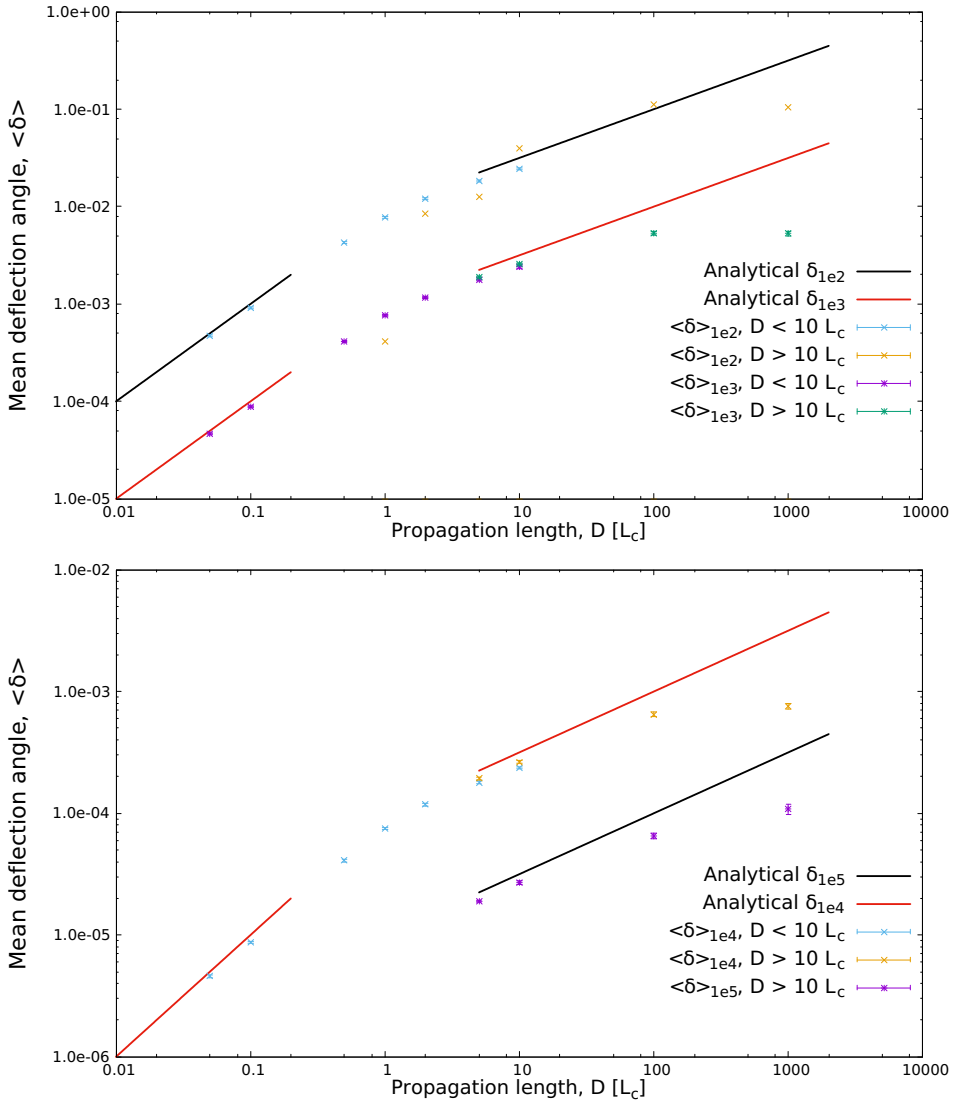

Figure 4.17: The plots show calculated deflection angles for electrons/positrons propagating through computed magnetic fields with spectral index $\gamma = 3.0$, relative turbulence scale size ratio $L_{\min}/L_{\max} = 0.01$, number of Fourier modes $n_k = 100$, and correlation length $L_c = 0.31$. $\langle\delta\rangle_x$ is the mean deflection angle for the electrons/positrons with gyroradius $R_g = x \cdot L_c$. The bars represent the standard error of the mean and the solid lines are the analytical expectation values in the limits of the propagation length $D \ll L_c$ and $D \gg L_c$ (see equations (3.5) and (3.6)).

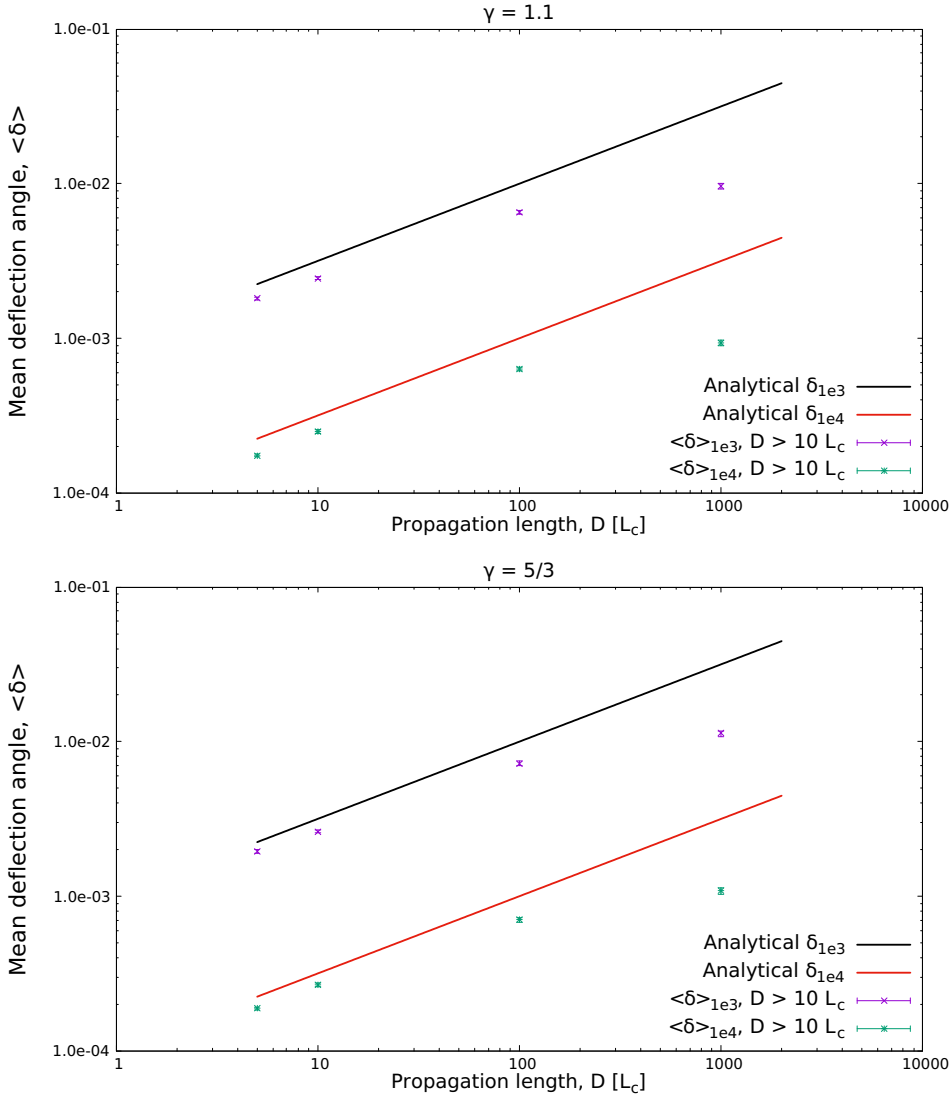

Figure 4.18: The plots show calculated deflection angles for electrons/positrons propagating through computed magnetic fields with different spectral indices γ at relative turbulence scale size ratio $L_{\min}/L_{\max} = 0.91$, with $n_k = 100$ Fourier modes, and correlation lengths $L_c = 0.40$ for $\gamma = 5/3$ and $L_c = 0.46$ for $\gamma = 1.1$. $\langle\delta\rangle_x$ is the mean deflection angle for the electrons/positrons with gyroradius $R_g = x \cdot L_c$. The bars represent the standard error of the mean and the solid lines are the analytical expectation values in the limit of the propagation length $D \gg L_c$ (see equation (3.6)).

Chapter 5

Conclusion

In this report a number of numerical computations of turbulent magnetic fields has been preformed, with goal of calculating the mean deflection angle of very high energy particles through random turbulent magnetic fields that are homogeneous, normalized with zero mean, and isotropic. The magnetic fields were computed with an algorithm presented in Giacalone and Jokipii (1994) which creates turbulent magnetic fields by modelling the fields as a superposition of Fourier modes. The wavenumbers k of the Fourier modes were spaced logarithmically between k_{min} and k_{max} and their propagation directions were randomly chosen with an isotropic probability distribution. The fields were set to follow a power spectrum $E \propto k^{-\gamma}$ and with a normalized strength of the magnetic field equal to B_{rms}.

The first part, the report shows through several numerical computations that any field computed by the algorithm approaches the correct normalization for the RMS value of the field strength, and a zero mean, at scale sizes $\gtrsim 10 L_{\text{max}} = 20\pi / k_{\text{min}}$. This is independent of γ, the $k_{\text{min}}/k_{\text{max}}$ ratio, and the number of Fourier modes per decade of k-values. Further the report finds that for a large number of modes per decade of k-values the computed field approached isotropy. With $\gamma = 5/3$, i.e. Kolmogorov turbulence, one needs 500 modes per decade to get a high degree of isotropy for a computed field. The MS value of the field components are then statistically spread ($\approx$ normal distribution) around a mean value of $1/3\ B_{\text{rms}}^2$, with a standard deviation of $\approx 5\%$ of the mean. Furthermore the report finds that a change in the number of modes per decade or the value of γ does not change the field components' MS value, but will change the standard deviation. A decreasing number of modes per decade or an increasing value of γ increase the STD, while an increasing number of modes per decade or a decreasing value of γ will decrease the STD. At 50 modes per decade the standard deviation increase to $\approx 13\%$ of the mean for $\gamma = 5/3$, while for 500 modes per decade and $\gamma = 5$ the STD is $\approx 10\%$, and for $\gamma = 1.1$ the STD is $\approx 2.5\%$. In addition, the report shows that the disagreement of Tautz (2012) on the question of the isotropy of the computed fields was the result of wrong probability distribution of the random angle θ for each wavevector $\boldsymbol{k}$.

In the second part, the report shows the calculated correlation lengths L_c of randomly generated magnetic fields and compares the results against the correlation lengths of equivalent analytical fields, i.e. homogeneous and isotropic with the same power law and normalization, but with continuous wavenumbers for the Fourier modes. For relative turbulence scale ratios $L_{\text{min}}/L_{\text{max}} = k_{\text{min}}/k_{\text{max}} > 0.5$ and spectral indices γ close to 1, the correlation lengths of the computed fields are shown to follow the analytical correlation length of the continuous fields.

One find that in the limit $L_{\text{min}}/L_{\text{max}} = 1$ the correlation length of a computed field goes towards $0.5L_{\text{max}}$, while at small ratios $L_{\text{min}}/L_{\text{max}} \ll 1$ the correlation length approaches a constant value in the range 0.0-0.5L_{max}. In general this value differ from what is expected from a continuous field. In addition the report finds that this constant correlation length for small scale ratios increase with increasing values of γ, but seams to decrease with an increasing number of modes per decade. Whether the degree of isotropy of the computed fields affect the correlation length is not explicitly proved in the report, but indications that higher degree of isotropy give more stable correlation lengths are shown.

In the third part of the report, the results from several numerical simulations of VHE electrons propagating through randomly generated magnetic fields are presented. The report finds that the mean deflection angles of electrons propagating through the computed magnetic fields follow the analytical formula for propagation lengths $D \ll L_c$, see equation (3.5). On the contrary the report finds that at longer propagation lengths $D \gg L_c$ the mean deflection angles deviate from the analytical expectations, see equation (3.6). In order for the deflection angles to match the expected values, one finds that the correlation lengths would have to be 10 times smaller than what was calculated in the second part of the report. In addition at propagation lengths $D > R_g$ the mean deflection angle approaches $\pi/2$ as the velocity directions approach isotropic distribution. This is due to the fact that the computational algorithm loses track of angles $\delta > \pi$ as it calculates the angle based on the initial and the current velocity at any given propagation length. The most probable sources of error for the deviations in deflection angles relative the analytical expectations are found to be the time increment of the Runge-Kutta solver in the propagation algorithm, and the computed fields isotropy. Both potential sources require additional testing with smaller time increments or more Fourier modes to be proved or disproved, but this requires more computation time than what is possible within the time window of the project presented in this report.

Appendix A

Acronyms

CR Cosmic rays

EBL Extragalactic background light

EGMF Extragalactic magnetic field

EMC Electromagnetic cascade

MC Monte-Carlo

MF Magnetic field

MS Mean square

RK Runge-Kutta

RMS Root mean square

SE Standard error

STD Standard deviation

VHE Very high energy

Bibliography

Bergström, L. and Goobar, A. (2004). *Cosmology and Particle Astrophysics*. Springer, Berlin, 2nd edition.

Caprini, C. and Gabici, S. (2015). Gamma-ray observations of blazars and the intergalactic magnetic field spectrum. *Phys. Rev. D*, 91:123514.

Durrer, R. and Neronov, A. (2013). Cosmological Magnetic Fields: Their Generation, Evolution and Observation. *Astronomy & Astrophyics Review*, 21:62.

Giacalone, J. and Jokipii, J. (1994). Charged-particle motion in multidimensional magnetic-field turbulence. *Astrophysical Journal*, 430(2 PART 2):L137–L140.

Giacalone, J. and Jokipii, J. (1999). The Transport of Cosmic Rays across a Turbulent Magnetic Field. *Astrophysical Journal*, 520(1):L204–L214.

Griffiths, D. J. (2014). *Introduction to Electrodynamics*. Pearson, Harlow, 4th edition.

Harari, D., Mollerach, S., Roulet, E., and Sánchez, F. (2002). Lensing of ultra-high energy cosmic rays in turbulent magnetic fields. *Journal of High Energy Physics*, 2002(03):045.

Hemmer, P. C. (2002). *Termisk Fysikk*. Tapir Akademisk Forlag, Trondheim, 2nd edition.

Neronov, A., Semikoz, D., Kachelriess, M., Ostapchenko, S., and Elyiv, A. (2010). Degree-scale GeV "jets" from active and dead TeV blazars. *Astrophysical Journal Letters*, 719(2 PART 2):L130–L133.

Neronov, A. and Semikoz, D. V. (2009). Sensitivity of γ-ray telescopes for detection of magnetic fields in the intergalactic medium. *Phys. Rev. D*, 80:123012.

Press, W. H., Teukolsky, S. A., Vetterling, W. T., and Flannery, B. P. (1997). *Numerical Recipes in Fortran 77*. Press Syndicate of the University of Cambridge, Cambridge, 2nd edition.

Tautz, R. C. (2012). On Simplified Numerical Turbulence Models in Test-particle Simulations. *Journal of Computational Physics*, 231(14):L4537–L4541.

Taylor, A. M., Vovk, I., and Neronov, A. (2010). Extragalactic magnetic fields constraints from simultaneous GeV-TeV observations of blazars. *Astronomy & Astrophysics*, 529:A144.